International Journal of Biological Macromolecules 342 (2026) 150368

Contents lists available at ScienceDirect

International Journal of Biological Macromolecules

journal homepage: www.elsevier.com/locate/ijbiomac

Chitosan-xanthan gum-based hydrogels loaded with essential oil distillation by-products of *Aloysia citrodora* Paláu for antimicrobial systems

Heloísa H.S. Almeida [a,b], Arantzazu Santamaria-Echart [a], Joana S. Amaral [a], Leandro L. Aquino [a], Alírio E. Rodrigues [b], Maria-Filomena Barreiro [a,*]

[a] CIMO, LA SusTEC, Instituto Politécnico de Bragança, Campus de Santa Apolónia, 5300-253, Bragança, Portugal
[b] LSRE-LCM, ALiCE, Faculty of Engineering, University of Porto, Rua Dr. Roberto Frias, 4200-465, Porto, Portugal

ARTICLE INFO

Keywords:
Chitosan
Xanthan gum
Hydrogel
Essential oil by-products
Waste valorisation
Hydrosols
Antimicrobial activity

ABSTRACT

Hydrogels, 3D hydrophilic networks formed by oppositely charged biopolymers like chitosan and xanthan gum, offer a safe, non-toxic, and biocompatible option for delivery applications. Essential oil (EO) by-products, such as hydrosols and wastewater, are sources of antioxidant and antimicrobial compounds, but their high dilution can limit direct applications. In this context, this work focused on the development of hydrogels via electrostatic complexation incorporating hydrosol and wastewater by-products from the steam distillation of *Aloysia citrodora* Paláu, using a two-stage approach: (a) initial loading during hydrogel formation and (b) subsequent reloading of the hydrogels to further enhance the concentration of bioactive compounds. The effect of pH (4, 7, and 11) on polymer complexation was evaluated, as it influences polymer-polymer and polymer-bioactive compound interactions by modifying the protonation and deprotonation states of their functional groups. This effect was evident in swelling, release kinetics, morphology, and rheological properties. Fourier-transform infrared (FTIR) analysis confirmed the successful formation of the polymer complex. Neutral pH hydrogels showed the highest hydrosol entrapment (70.3%) and were selected as the most promising systems. Biological characterisation showed that the reloading process enhanced bioactivity. Wastewater-load-reload improved antioxidant capacity, driven by the high phenolic content. Moreover, hydrosol-loaded-reload systems exhibited antimicrobial activity, with bactericidal effects against *Staphylococcus aureus* and *Escherichia coli*, outperforming both unloaded and loaded systems. These findings highlight the potential of loading and reloading steps to valorise EO by-products, producing sustainable, functional hydrogels with high bioactivity, suitable for food, pharmaceutical, medical, and biotechnological applications.

1. Introduction

Interest is growing in developing innovative biobased antimicrobial systems as alternatives to conventional pharmaceuticals and preservatives, aiming to combat the resilience and survival of microorganisms exposed to antimicrobial agents [1,2]. Pathogenic bacteria such as *Staphylococcus aureus* (Gram-positive) and *Escherichia coli* (Gram-negative) are widely distributed across different environments. They are major contributors to infections due to their biofilm-forming capabilities, resistance, virulence factors, and toxin secretion [3]. In this context, hydrogel systems have attracted attention for their versatility, serving as a base material for a range of applications.

Hydrogels are flexible, three-dimensional hydrophilic networks that retain water without dissolving, presenting high stretchability and easy shaping [4]. Among various approaches, networks can be created through the interactions of oppositely charged polymers, a safe and eco-friendly method, to form polyelectrolyte complexes (PECs). PECs are formed spontaneously through the ionic complexation of mixed polyelectrolyte solutions without using organic solvents, chemical cross-linkers, or surfactants [5]. Polysaccharides, composed of monosaccharide units linked by glycosidic bonds, are a key class of natural polymers valued for their nontoxicity, biocompatibility, and biodegradability. Their abundant functional groups enable them to activate their ionic character, promoting PEC formation [6,7].

Chitosan (CH), the only cationic polysaccharide, is a linear polymer composed of β-(1,4)-linked D-glucosamine and *N*-acetyl-D-glucosamine units, obtained through the deacetylation of chitin [5]. This distinctive molecular structure, comprising glucosamine units, endows chitosan

* Corresponding author at: Instituto Politécnico de Bragança, Campus de Santa Apolónia, 5300-253, Bragança, Portugal.
E-mail address: barreiro@ipb.pt (M.-F. Barreiro).

https://doi.org/10.1016/j.ijbiomac.2026.150368
Received 19 September 2025; Received in revised form 10 January 2026; Accepted 17 January 2026
Available online 19 January 2026

with exceptional biological properties [4]. Xanthan gum (XG) is a naturally water-soluble polysaccharide produced during the fermentation of *Xanthomonas campestris* bacteria. It has a high molecular weight and comprises a β-1,4-linked glucan backbone, with charged trisaccharide side chains attached to alternating glucose residues. Acetate and pyruvate groups on its backbone make XG an anionic polysaccharide [8]. Due to their oppositely charged chains, CH and XG can form PECs at certain pH values via electrostatic self-crosslinking, creating a biocompatible, non-toxic natural polymeric network that is ideal for controlled-release systems.

Plant-derived extracts, rich in bioactive compounds such as carotenoids, phenolic acids, flavonoids, alkaloids, saponins, and terpenoids, among others, exhibit various biological activities, including antibacterial, antifungal, antioxidant, and anti-inflammatory effects [9]. However, their instability and sensitivity to external conditions can limit their use, making protective strategies essential. In this regard, encapsulation has proven to be an effective method for preserving their activity and enhancing targeted delivery [10]. *Aloysia citrodora*, or lemon verbena, is a perennial herb in the Verbenaceae family, renowned for its aromatic characteristics and high essential oil (EO) content. It is commonly used in aromatherapy, perfumery, and as a food flavouring ingredient [11]. Its EO is recognised for its antimicrobial, anti-inflammatory, and anti-tumour properties, making it a valuable source of bioactive compounds [12].

Despite its global relevance, high citral content, and generally recognised as safe (GRAS) status, the characterisation and exploitation of *A. citrodora* distillation by-products remain limited, as research has predominantly focused on extracting essential oil and polyphenols [13,14]. EO distillation yields rarely exceed 5%, leaving more than 95% of the plant material as residual biomass, plus the hydrosol and wastewater, which are often discarded without treatment. Therefore, valorising these residues is a key strategy to enhance the environmental and economic sustainability of the EO industry [15,16].

Hydrosols, secondary products of EOs' extraction, are complex mixtures of diluted hydrophilic bioactive compounds, containing trace amounts of hydrophobic constituents from EOs. Due to their complex composition, the bioactivity of these compounds is linked to functional groups such as methyl, hydroxyl, carbonyl, and carboxyl [17,18]. Solid residues and wastewater also exhibit complex compositions, containing high-molecular-weight water-soluble compounds, mainly polyphenolic compounds [19]. In this context, the high dilution of bioactives in the distillation by-products makes encapsulation in hydrogels effective for concentrating and protecting compounds, enhancing bioavailability, and enabling direct use in green antimicrobial systems.

This study focuses on developing functional hydrogel systems based on the electrostatic complexation of chitosan and xanthan gum to entrap and concentrate bioactive compounds derived from *A. citrodora* distillation by-products, namely hydrosols and wastewater. The influence of pH on hydrogel formation was investigated, and hydrogel characterisation included physicochemical, structural, rheological, and release analyses, along with bioactivity evaluations using antioxidant and antimicrobial assays against *S. aureus* and *E. coli*. A reloading strategy was implemented to increase the accumulation of bioactive compounds within the hydrogel matrix, highlighting the novelty of these systems in valorising essential oil by-products and enhancing the biological activity of the resulting products.

2. Materials and methods

2.1. Materials

Fresh plant (*Aloysia citrodora* Paláu) supplied by Deifil Technology Lda (Póvoa de Lanhoso, Portugal) was received, cut, frozen, and stored at −20 °C (Hotpoint-Ariston, Italy). Chitosan (CH; deacetylation degree of 85%, viscosity of 10 mPa·s for 1% solution in acetic acid (1%), ash content <1%) obtained from BioLog (Heppe GmbH, Landsberg, Germany) and xanthan gum (XG; viscosity of 1.45 to 2.00 mPa·s for 1% solution at 20 °C) acquired from TCI Europe (Zwijndrecht, Belgium) were chosen as polymers used in the hydrogels. Citric acid (99%), methanol (99.8%), and sodium hydroxide were obtained from Merck Millipore (Darmstadt, Germany), Riedel-de-Haën (Honeywell, Germany), and Sigma-Aldrich (Merck, Germany), respectively. For the antioxidant activity, free radical solutions were prepared using ABTS (2,2′-azino-bis-3-ethylbenzothiazoline-6-sulfonic acid) and DPPH (2,2′-diphenyl-1-picrylhydrazyl) obtained from Sigma-Aldrich (St. Louis, MO, USA). The microbial cultures selected in this study included the bacteria *Staphylococcus aureus* ATCC 6538 and *Escherichia coli* ATCC 8739, both purchased from Mistracon (Sharlab, Spain). The microorganisms' substrates, brain-heart infusion (BHI) broth and nutrient agar, were purchased from Liofilchem (Italy). Distilled water was used for all the conducted experiments.

2.2. Hydrosol and wastewater production

The *A. citrodora* by-products, hydrosols (H) and wastewater (W) were obtained by steam-distillation. Briefly, 100 g of the plant material was placed in a cylindrical flask connected to the water vapour distillation flask, where the vapourised water interacted with the plant, carrying a complex mixture of vapourised water and oil. After 1.5 h of distillation, the EO and its respective by-products (H and W) were separated and collected, then stored at refrigerated conditions. Their complete characterisation was previously reported in a work of the group [20]. Briefly, the samples presented an acidic pH (H = 5.96 and W = 5.42) and a strong odour. The main composition of the H consisted of the citral isomers, namely neral (31.21%) and geranial (36.69%), and also showed a lower content of phenolic compounds (20.5 μg/mL in the hydrosol). The W presented a high content of phenolic compounds (120.0 μg/mL wastewater), including luteolin-7-diglucuronide (39.7 μg/mL wastewater), forsythoside H (13.8 μg/mL wastewater), and apigenin-7-diglucuronide (13.1 μg/mL wastewater), as main compounds.

2.3. Hydrogel preparation

For the preparation of the hydrogels, two polymeric solutions (CH and XG) were prepared using an adapted procedure from Martínez-Ruvalcaba et al. [21], with some modifications, including the use of the *A. citrodora* by-products (H and W) in the forming solutions. The CH solution (1% *w/v*, total volume 100 mL) was prepared by dissolving the CH in a 2% (*w/v*) citric acid solution, stirred magnetically at 60 °C (overnight) until complete dissolution. XG dissolution was achieved at room temperature under magnetic stirring at 1% (*w/v*) polymer concentration, with a total volume of 100 mL. The distilled water used for the XG solutions was substituted with H or W to load the hydrogels with the bioactive waste products during preparation (H and W were added directly, without dilution). To cover different XG pH environments, which influence the polymer's net charge, the pH was adjusted to 4, 7, and 11 using 2% (*w/v*) citric acid and 0.5% (*w/v*) sodium hydroxide. To form the hydrogels, the resultant CH- and XG-based solutions were mixed and stirred (250 rpm) for 10 min at room temperature, and the formed hydrogel was recovered by filtration. Each hydrogel was freeze-dried (48 h, −106 °C, 5×10^{-4} mbar) (Labogene, ScanVac CoolSafe, Lillerod, Denmark). The lyophilised hydrogels were stored under refrigerated conditions (4 °C) before further analysis.

The produced hydrogels were designated as base hydrogels and labelled using the following nomenclature: XY, where X refers to the used by-product (H, W, and C when distilled water was used for comparative purposes), and Y is the final pH environment of the XG sample (a-acid (pH 4), b-basic (pH 11), and n-neutral (pH 7)). For example, sample Ha corresponds to the hydrogel formed using the XG solution prepared with the hydrosol at acidic conditions.

2.4. Hydrogel characterisation

The prepared base hydrogel systems were characterised for their chemical structure to assess CH-XG interactions, H and W entrapment, swelling, and release, as well as morphology and rheological properties.

To investigate the chemical structure and CH-XG molecular interactions, and to evaluate the entrapment effects resulting from polymer-bioactive compound interactions, Fourier-transform infrared (FTIR) spectroscopy was performed using an MB3000 FTIR spectrometer (ABB, Zurich, Switzerland) operating in attenuated total reflectance (ATR) mode. The cell was equipped with a diamond crystal. The following parameters were used: 32 scans at a resolution of 4 cm^{-1} in the range from 4000 to 550 cm^{-1}. The spectra were acquired and processed with Horizon MB version 3.4. A small sample of each lyophilised hydrogel was placed directly on the crystal surface for the analysis.

The H and W entrapment (ET) capacity of the produced hydrogel systems was estimated using an indirect method [22]. After forming and separating the hydrogel by filtration, 1 mL of the residual solution was diluted (1:10) with water, then analysed using a UV–Vis spectrophotometer (Cary 50, Varian, Australia). Quantification was performed by measuring absorbance at the maximum wavelengths (243 nm for H and 328 nm for W). The calibration curves for both by-products (Supplementary Material) showed high correlation coefficients (R^2 values of 0.9997 and 1, respectively). ET was calculated according to Eq. (1).

$$ET\ (\%) = \left(\frac{W_t - W_f}{W_t}\right) \times 100 \quad (1)$$

where W_t is the total weight of H or W added to the hydrogel preparation system (measured gravimetrically), and W_f is the amount of H or W in the residual solution, estimated by UV–Vis.

The swelling capacity of the lyophilised hydrogels was determined gravimetrically. Dried samples (0.05 g) were immersed at room temperature in distilled water (15 mL), and the swelling was measured by weighing the swollen hydrogel over time until constant weight was achieved. The swelling ratio (SR) was calculated using Eq. (2).

$$SR\ (\%) = \left(\frac{W_s - W_l}{W_l}\right) \times 100 \quad (2)$$

where W_s and W_l refer to the weight of the swollen and lyophilised hydrogel, respectively.

Following, the swelling kinetics was analysed using the Korsmeyer–Peppas model (Eq. (3)). The model was applied to the initial swelling stage, with a fitting range of $M_t/M_\infty \leq 0.8$ to ensure statistical robustness [23].

$$\frac{M_t}{M_\infty} = kt^n \quad (3)$$

where M_t and M_∞ represent the amounts of water absorbed at time t and at equilibrium, respectively, k is a kinetic constant related to the swelling rate, and n is the swelling mechanism exponent. Specifically, $n < 0.5$ indicates a pseudo-Fickian diffusion mechanism, $n = 0.5$ corresponds to Fickian diffusion, while $0.5 < n < 1$ represents a non-Fickian (anomalous) mechanism.

To investigate the hydrogel's morphology, scanning electron microscopy (SEM) coupled with energy-dispersive X-ray spectroscopy (EDS) was performed using a high-resolution Schottky field-emission environmental scanning electron microscope (FEI Quanta 400 FEG ESEM), equipped with X-ray microanalysis and electron backscattered diffraction (EBSD) capabilities (EDAX Genesis X4M system). Dried hydrogel samples were attached to carbon tape and sputter-coated with a thin gold–palladium (Au/Pd) layer using an SPI module sputter coater. Coating was carried out for 100 s at 15 mA to ensure adequate surface conductivity.

2.5. Hydrogel reloading

A reload step for the base systems with H or W was tested using the swelling-diffusion technique to enhance the hydrogels' activity. Briefly, freeze-dried hydrogel systems (0.05 g) were immersed directly in H or W (10 g, without dilution) for 3 h at room temperature, as determined by the swelling capacity analysis. This facilitated the penetration of the bioactive components into the hydrogel structure and their adsorption at the surface. The swollen hydrogels were filtered, frozen, and lyophilised, then stored at 4 °C for further analysis. The designation +Z was added to the previous nomenclature of the base hydrogels to highlight the reload step. For example, sample Ha + H corresponds to the base hydrogel Ha subjected to a reload step with H. The reloading capacity (RC%) of the hydrogel using H or W was determined gravimetrically using Eq. (4).

$$RC\ (\%) = \left(\frac{W_b - W_r}{W_h + W_b}\right) \times 100 \quad (4)$$

where W_b is the total weight of the by-product (H or W) used in reloading, W_r is the weight of residual solution after reloading, and W_h is the initial weight of the lyophilised hydrogel.

To investigate the release capacity of loaded and reloaded hydrogel systems for H- or W-bioactive compounds, a cumulative release assay was performed in triplicate under controlled conditions. Dried samples (0.1 g) were immersed in distilled water (30 g) under continuous stirring (100 rpm) in a shaker-incubator (ES-20/80, BioSan, Latvia) at 25 °C. At different time intervals (0.2, 1, 2, 4, 6, and 8 h), aliquots of 3 mL were collected, and the released H or W was measured using a UV–Vis spectrophotometer (Cary 50, Varian, Australia) at 243 nm for the H and 328 nm for the W. The aliquots were then returned to maintain the total volume. The concentration of the released H or W at each time point (C_t) was calculated according to Eq. (5). The corresponding mass of the released hydrosol or wastewater (m_t) was calculated as:

$$m_t = C_t \times V \quad (5)$$

where V is the volume of the release medium.

The cumulative release was normalised with respect to the dry mass of the hydrogel sample and expressed as milligrams of released hydrosol or wastewater per gram of dry hydrogel (m_{dry}; mg/g), according to Eq. (6):

$$M_t = \frac{m_t}{m_{dry}} \quad (6)$$

where M_t is the cumulative amount of released H or W at time t.

The compounds' release from the hydrogel matrices is influenced by multiple factors, as swelling plays a key role in diffusion-mediated release. The release patterns were analysed using the pseudo-first-order (Eq. (7)), Higuchi (Eq. (8)), and Korsmeyer–Peppas (Eq. (3)) models [24].

$$\ln(M_\infty - M_t) = \ln(M_\infty) - k_1 t \quad (7)$$

where M_t is the amount of H or W released at time t, M_∞ is the maximum experimental release, and k_1 is the pseudo-first order rate constant.

$$M_t = k_H t^{1/2} \quad (8)$$

where M_t is the amount of H or W released at time t, and k_H is the Higuchi constant.

In the Korsmeyer-Peppas model, M_t and M_∞ represent the amounts of H or W released at time t and at equilibrium, respectively; k is the release rate constant; and n is the release mechanism exponent. Specifically, $n = 0.45$ indicates a Fickian diffusion mechanism, while $n > 0.45$ but <1 indicates a non-Fickian (anomalous) transport mechanism.

The rheological characterisation was evaluated using a rotational Rheometer Kinexus Prime lab+ (NETZSCH, Germany). The rheological properties of hydrogels include viscosity (measured via flow tests) and

dynamic properties, such as frequency- and amplitude-sweep tests. Samples for rheological measurements were rehydrated by adding the freeze-dried hydrogel to distilled water, allowing it to swell completely (3 h). Assays were carried out at 25 °C using a parallel-plate geometry with a 20 mm diameter and a 1 mm gap. Flow tests were performed by increasing the shear rate from 10^{-3} to 10^{2} s^{-1}. The amplitude and frequency sweeps were carried out over shear strain (%) between 10^{-1} and 10^{2}% and frequency (Hz) between 10^{-1} and 10^{1} Hz with a fixed shear strain in the linear viscoelastic region (LVR).

2.6. Antioxidant activity: ABTS and DPPH assays

The antioxidant activity of the base and reloaded hydrogels was evaluated through the discoloration and neutralisation of ABTS (2,2′-azino-bis-3-ethylbenzothiazoline-6-sulfonic acid) and DPPH (2,2′-diphenyl-1-picrylhydrazyl) free radicals using spectrophotometric methods with adaptations [25]. For both assays, samples were prepared at a hydrogel-to-water ratio of 1:200 (*w/w*) and stirred for 15 min. Distilled water was used as the control. For the DPPH assay, serial dilutions were prepared by adding 30 μL of the hydrogel solution, followed by 270 μL of the DPPH methanolic solution. The samples were kept in the dark for 1 h and then analysed by spectrophotometry (Epoch, BioTek Instruments, USA) at 517 nm. For the ABTS assay, 150 μL of the hydrogel solution were added to 4.85 mL of the ABTS solution. The samples were kept in the dark for 15 min and then analysed by spectrophotometry (V-730 UV–visible, Jasco, Madrid, Spain) at 734 nm. Samples' scavenging capacity (SC%) was calculated using Eq. (9).

$$SC(\%) = \left(\frac{A_c - A_s}{A_c}\right) \times 100 \tag{9}$$

where A_C is the absorbance of the control, and A_S is the absorbance of the sample.

To assess the effect of the reload step and its direct influence on the antioxidant activity, for W-reloaded hydrogels, total phenolic and flavonoid contents were determined and compared with those of the base systems prepared with H and W. Briefly, hydrogel solutions (5 mg/mL) were prepared, the phenolic content was measured by the Folin-Ciocalteu assay (765 nm) and the flavonoid content by the aluminium chloride assay (510 nm) following Barros et al. [26], with absorbances recorded using a microplate reading (Epoch, BioTek Instruments, USA). Results were expressed as mg gallic acid or mg catechin equivalents per gram. Distilled water was used as a blank, and calibration curves showed a high correlation (Supplementary Material).

2.7. Antimicrobial activity

The microbial cultures of *Staphylococcus aureus* ATCC 6538 and *Escherichia coli* ATCC 8739, stored in an ultra-freezer (ThermoFisher, STP, AS) at −70 °C, were activated in BHI broth and incubated for 24 h at 37 °C in a bacteriological oven (Raypa, Incutterm, Barcelona, Spain). The inoculum was then prepared in BHI broth by standardising the cell density suspension at 550 nm in a densitometer (DEN-1 McFarland densitometer, Grant-bio, UK) to achieve a final cell density of 1.5×10^{8} cells/mL.

The antimicrobial potential of the hydrogels was determined using the neutral systems (Cn, Hn and Wn) and two reloaded neutral systems (Hn + H and Wn + H), chosen following preliminary tests (viable cell counting method and agar diffusion assay; described in the Supplementary Material) that pointed out the neutral systems prepared with H as the most promising, considering antimicrobial activity. The samples underwent microbial reduction assay using a standard method under dynamic contact conditions, adapted from Fernandes and co-workers [27]. Briefly, the standardised inoculum (1.5×10^{8} cells/mL) was diluted in sterile buffer (0.3 mM KH_2PO_4, pH = 7.2 ± 0.1) to obtain a working bacterial dilution for the assay, resulting in a final concentration of 1.5×10^{5} cells/mL. For antimicrobial activity evaluation, 333 mg of each lyophilised hydrogel was added to a sterile 100 mL flask containing 50 mL of the working bacterial dilution. The flasks were placed in a shaker-incubator (ES-20/80, BioSan, Latvia) at 37 °C and 100 rpm. After 1 min of stirring, 1 mL of the solution was aseptically collected to determine the bacterial concentration using the viable cell counting technique (via serial dilutions and the agar incorporation method in Petri dishes with nutrient agar). This sampling represented the bacterial concentration at the initial contact time (t0). After sampling, the flasks were immediately returned to the shaker incubator. This aseptic sampling step was repeated at different time points, namely 0.5, 1, 2, 4, 6, and 8 h (representing the t0.5, t1, t2, t4, t6, and t8 contact times). A flask containing only the working bacterial dilution (without hydrogel addition) was analysed in parallel as the control. The colony-forming unit (CFU) counts were converted to CFU/mL and used to calculate the bacterial decimal reduction (DR) and the percentage reduction (PR%), using Eqs. (10) and (11).

$$DR = \log\frac{C_0}{C_t} \tag{10}$$

where C_0 represents the initial CFU count, and C_t refers to the CFU count at time t following the contact period with the sample.

$$PR(\%) = \left(1 - \frac{1}{10^{DR}}\right) \times 100 \tag{11}$$

where DR is the decimal reduction calculated using Eq. (10).

A concise schematic summarising the hydrogel synthesis, loading, reloading, and the hydrogel's chemical and biological characterisation is presented in Fig. 1, providing an overview of the experimental workflow and proposed antimicrobial and antioxidant mechanisms.

2.8. Statistical analysis

Results were reported as mean ± standard deviation of replicates ($N = 3$). Data were analysed using ANOVA with Tukey's multiple comparison test in GraphPad Prism® 8.0 (San Diego, CA, USA) when applicable. Kinetic model fitting was conducted in RStudio (version 4.3.0) using linear regression on transformed data. Model performance was evaluated using the coefficient of determination (R^2), and the most appropriate kinetic model for each hydrogel system was selected based on the highest R^2 and the physical relevance of the fitted parameters.

3. Results and discussion

3.1. Hydrogel formation

Fig. 2 illustrates the schematic representation of the hydrogel formation process. The effective formation of PECs depends on various conditions, including polymer concentration, polymer ratio, and pH. Regarding pH, for effective polymer complexation, the pH of the polymeric solutions should be far from the polymers' pKa values (lower than 6.5 for CH and higher than 3.1 for XG) to ensure the activation of functional groups and subsequent electrostatic interactions upon contact [5,28–30]. CH-XG hydrogels contain two ionisable functional groups: the carboxyl group (anionic) from XG and the amino group (cationic) from CH. The oppositely charged functional groups form electrostatic interactions that lead to hydrogel formation and stabilisation, with hydrogen bonding playing a significant role in stabilising the formed polyelectrolyte complexes. This combination of forces allows the hydrogel to remain stable over a broader pH range [31].

Besides polymer-polymer interactions, polymer-bioactive compound interactions can also be significant. Both by-products are complex mixtures; the hydrosol predominantly contains oxygenated monoterpenes, including citral, an acyclic monoterpene aldehyde, while the wastewater primarily consists of phenolic compounds characterised by

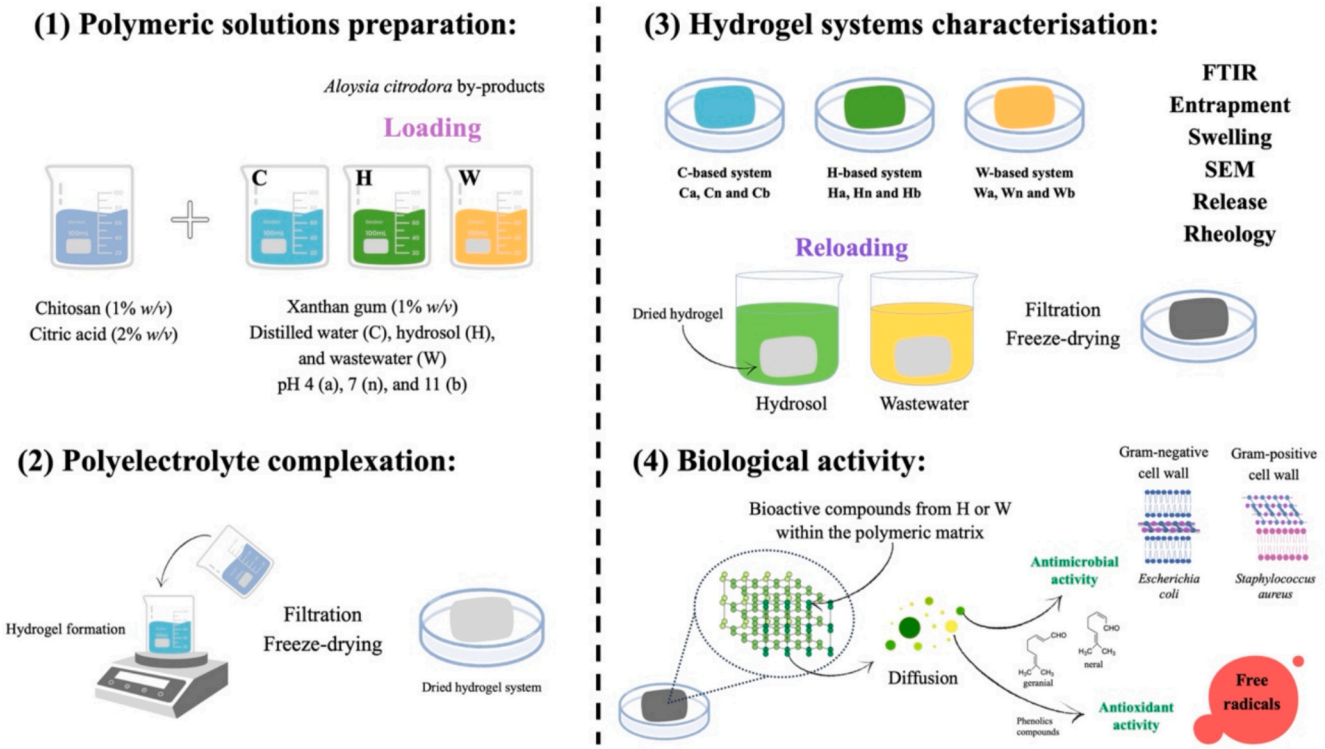

Fig. 1. Overview of hydrogel preparation and bioactivity mechanisms (Scheme made using Canva).

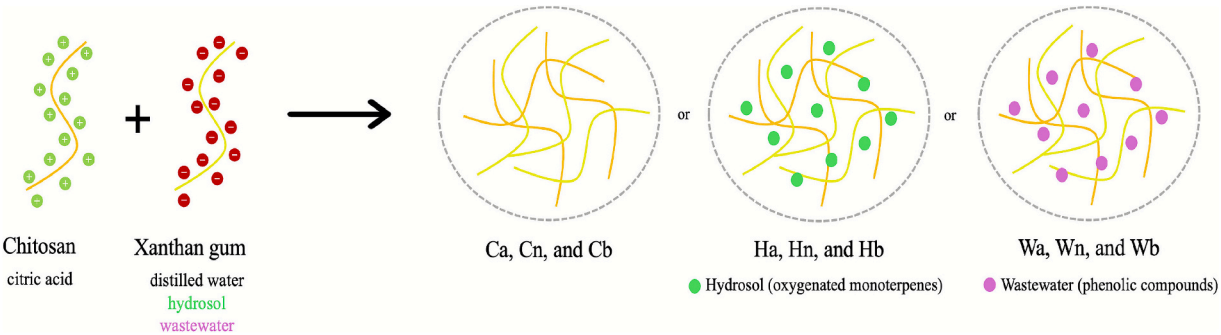

Fig. 2. Schematic representation of the polyelectrolyte complex formation with and without the hydrosol and the wastewater.

aromatic rings and hydroxyl groups. Interactions such as hydrogen bonding, ionic, and hydrophobic interactions may occur between the bioactive compounds and the polymer, trapping them more effectively within the hydrogel network and also helping to form a more stable polymeric matrix [32–34].

The CH solution, prepared with citric acid, achieved a pH of 2.70, facilitating the dissociation of chitosan's ionisable groups and making the functional groups available for electrostatic interactions. In addition to its biocompatibility, the citric acid used in the CH solution exhibits promising properties, including the ability to facilitate the grafting and conjugation of macromolecules. Its carboxylic and hydroxyl groups participate in hydrogen bonding interactions, which is beneficial when incorporating bioactive compounds into the polymeric network [35]. The XG solutions were adjusted to pH 4, 7, and 11 to investigate how pH affects ionisation levels and, consequently, complexation with CH. At pH 4, carboxyl groups are partially protonated, and XG chains maintain a double helix in concentrated solutions, transitioning to disordered coils as pH rises. At pH 6, carboxyl groups are fully deprotonated. In alkaline solutions, this deprotonation causes repulsion among negatively charged ions [36,37].

Polymer-bioactive compound interactions depend on several factors. In the case of the by-products used in this work, H and W, the interactions between the polysaccharides and aroma compounds associated with H, such as citral, may occur via hydrophobic interactions and hydrogen or covalent bonding [38]. Regarding phenolic compounds, which are mainly associated with W, non-covalent interactions can modify their structure, function, and biological activities [39]. Since phenolic compounds possess multiple hydrogen-bonding sites and are pH-dependent, they can, in some cases, influence electrostatic repulsion between molecules and modify the crystallinity of the polymeric matrix [40,41]. In summary, pH can also influence interactions between H and W compounds within the hydrogel structure, particularly by affecting the ionisation of functional groups and the availability of active sites for bonding and entrapment.

After the polymer complexation, all the produced systems exhibited similar weights. Visually, the lyophilised systems displayed a porous structure with a colour variation dependent on the used by-product, as illustrated in Fig. 3.

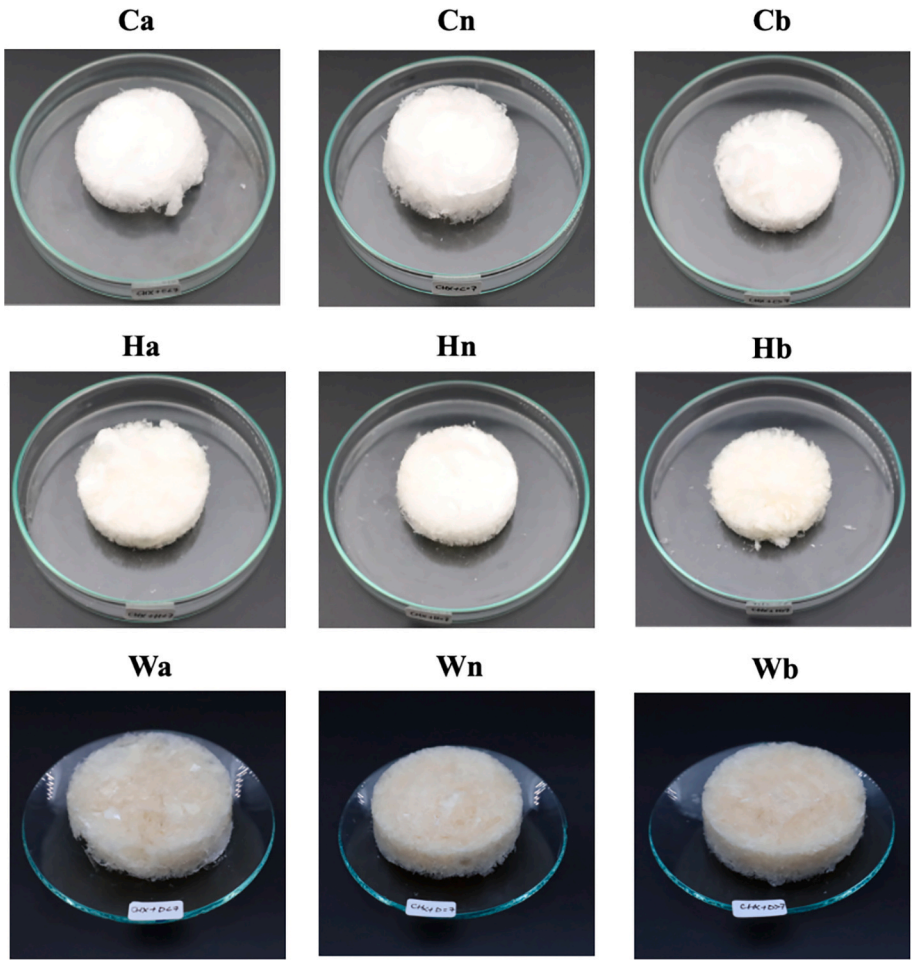

Fig. 3. Developed hydrogels with pH variation incorporating essential oil by-products: control (Ca, Cn, and Cb), hydrosol-based (Ha, Hn, and Hb) and wastewater-based (Wa, Wn, and Wb) systems.

3.2. Hydrogel characterisation

3.2.1. Fourier-transform infrared spectroscopy

The FTIR spectra of the analysed hydrogels (Fig. 4) were similar, presenting the characteristic vibration bands of CH and XG polymers. The CH spectrum (Fig. 4 (A)) exhibited a broad band around 3200–3300 cm^{-1}, indicative of —OH groups overlapped with —NH stretching vibrations [42]. A peak at 2800–2900 cm^{-1} was attributed to C—H stretching vibration, while the distinctive vibrations at 1650, 1580, and 1320 cm^{-1} were associated with the stretching of carbonyl (amide-I), N—H (amide-II), and the C—N (amide-III) bonds, respectively [31,43]. The symmetric bending vibrations of CH_2 and CH_3 were observed at 1425 and 1374 cm^{-1}, respectively. The band at 1150 cm^{-1} corresponded to the symmetric stretching of the C—O—C bond. The bands at 1020 and 1060 cm^{-1} were also assigned to the C—O stretching vibrations [42,44]. In the case of the XG, the spectrum featured a broad band associated with the —OH stretching at 3300 cm^{-1}, followed by the C—H stretching vibrations around 2900 cm^{-1} [45]. The signal around 1720 cm^{-1} corresponded to the C═O stretching of the carboxylic acids [46]. Vibrations at 1605 and 1400 cm^{-1} were attributed to the symmetric and asymmetric stretching of carboxylate groups (—COO—), while the band at 1020 cm^{-1} was associated with the C—O—C stretching vibrations [42,46].

Compared to the individual CH and XG spectra, the base hydrogels prepared with distilled water (Fig. 4 (B)) were similar, but with band shifts and the disappearance of signals between 1100 and 1700 cm^{-1}, associated with the amino, carboxyl, and hydroxyl groups. The observed shifts indicated polymer complexation resulting from interactions between the anionic and cationic charged groups [31,47,48]. Across all systems, the band observed at 1317–1370 cm^{-1} showed slight variations and was attributed to C—H vibrations of —$NHCOCH_3$ groups, confirming the presence of CH. The characteristic band at 1712–1720 cm^{-1} corresponded to the C═O stretching of the carboxylic acid moieties in XG. Together, these spectral features supported the occurrence of interactions between CH and XG, consistent with electrostatic attraction between the —NH_3^+ and the —COO^- groups [49]. Additionally, modifications in the 3000–3600 cm^{-1} region, attributed mainly to —OH stretching, suggested changes in hydrogen-bonding intensity, as evidenced by the band broadening. More complex spectra were observed for the base systems prepared with the by-products H and W (Fig. 4 (C) and (D), respectively). Shifts in the bands between 1100 and 1700 cm^{-1} and the appearance of new ones suggested interactions between functional groups and may correspond to the intrinsic vibrations of the bioactives, confirming their presence in the hydrogel matrix. In the H-based systems (Ha, Hn, and Hb) (Fig. 4 (C)), pH effects were discernible for Ha and Hb, reflected in the vibrations between 1060 and 1608 cm^{-1}. These vibrations correspond to the volatile compounds, including alkenes (C═C stretch), aromatics (C—C stretch), alkanes (—CH_3 stretching), and carboxylic acids (C—O stretch). Additionally, —CH_2 deformation modes around 1381 cm^{-1} indicated the presence of aldehydes, consistent with the citral molecule's structure, the major compound in H [50–52]. The neutral system (Hn) showed fewer peaks, indicating stronger interactions and more effective entrapment of bioactive compounds. Slight shifts in the band positions for the Hn

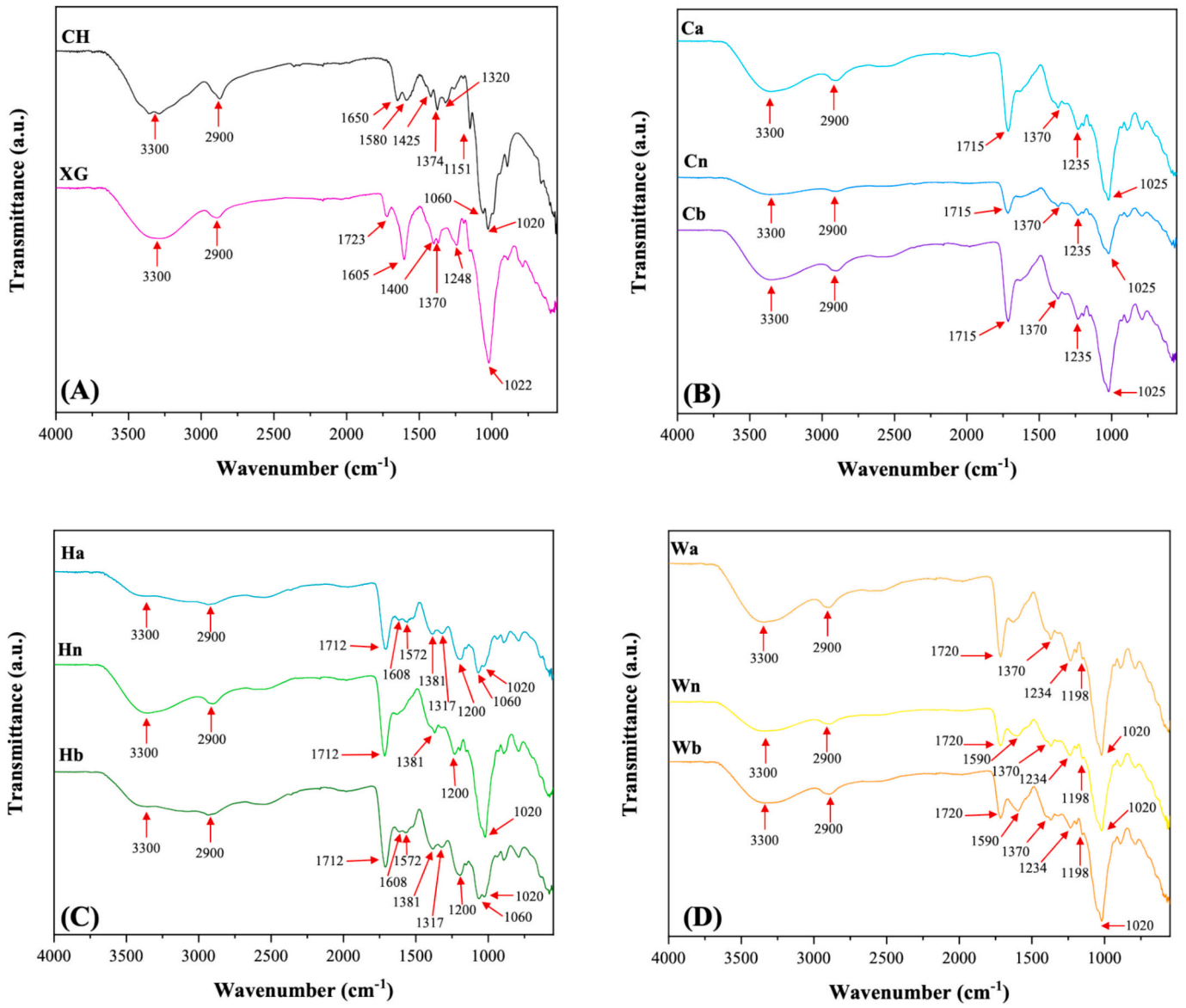

Fig. 4. FTIR spectra of the (A) CH and XG polymers, (B) control hydrogel systems (Ca, Cn, and Cb), (C) hydrosol-based systems (Ha, Hn, and Hb), and (D) wastewater-based systems (Wa, Wn, and Wb). Arrows indicate the assignment of the FTIR main vibration bands.

system further indicated citral's encapsulation within the system. The W-based systems (Wa, Wn, and Wb) (Fig. 4 (D)) also exhibited band shifts relative to the C-based systems, indicating interactions and the entrapment of bioactive compounds. Signals at 1590 cm^{-1} (C═C ring stretching) and 1198 cm^{-1} (C—OH stretching) correspond to the characteristic bands of flavonoids, specifically luteolin-7-diglucuronide, the W main component [53,54]. Similarly, the reloaded systems presented the same trend as the initially loaded systems (Supplementary Material). Systems reloaded with H, namely the neutral H- and W-based systems (Hn + H and Wn + H), also evidenced the entrapment of bioactive components, with characteristic peaks, further supporting the hydrogel matrix's entrapment capacity.

3.2.2. *Hydrosol and wastewater entrapment*

H and W entrapment represents the percentage of each by-product incorporated into the polymeric network. It is essential to have high values for effective functional hydrogels, such as antimicrobial systems [55]. Table 1 provides the values obtained for the hydrogels produced in the presence of H or W.

The hydrogel systems containing *A. citrodora* hydrosol showed the highest entrapment capacity, with Hn achieving the highest value (70.29%). This indicates an enhanced affinity of polymer-bioactive compounds, with substantial penetration of H into the hydrogel network, including the citral compound. Citral can act as a natural cross-linking agent due to its aldehyde functional group, by reacting with the amino groups of chitosan to form reversible imine (Schiff base) bonds. Along with physical entrapment within the CH-XG network, this

Table 1
Hydrosol and wastewater entrapment (ET%) of hydrogel systems produced in the presence of *A. citrodora* hydrosol and wastewater.

Hydrosol-based hydrogel systems	ET (%)	Wastewater-based hydrogel systems	ET (%)
Ha	62.07	Wa	1.56
Hn	70.29	Wn	5.49
Hb	69.27	Wb	36.42

ET = hydrosol and wastewater entrapment in the hydrogel matrix; Ha, Hn, Hb and Wa, Wn, Wb denote samples, where is H = hydrosol, W = wastewater, and a, n, b = final pH (acidic: 4, neutral: 7, basic: 11).

mechanism could promote a more stable hydrogel matrix and increase citral retention [56,57]. Afzal and co-workers [34] also studied citral entrapment in a chitosan-alginate hydrogel system prepared through electrostatic complexation. Using a 1:1 polymer ratio, they reported entrapment efficiencies of 68.1%, 71.5%, and 67.1% at pH 4, 7, and 10, respectively, which are comparable to those observed in the present study. In contrast, wastewater-based systems exhibited the lowest entrapment capacity due to pH-dependent protonation, which modifies interactions between polymers and bioactive components. At low pH, protonated xanthan gum and strong phenolic binding enhance hydrogen bonding, restricting effective entrapment and promoting aggregation rather than homogeneous network formation [58]. Studies have shown that non-covalent interactions between polysaccharides and polyphenols can induce aggregation and influence network stability [40,59]. At neutral pH, these interactions are partially reduced, though aggregation persists, resulting in moderate entrapment. At high pH, flavonoid deprotonation occurs, increasing the number of active sites and thereby enhancing interactions [60]. This pH effect led to varying entrapment capacities, with the alkaline Wb system demonstrating the highest capacity among the three studied systems (Wa, Wn, and Wb). From a circular valorisation perspective, adding 100 g of by-product per formulation was most effective for the H-based systems, which retained the highest by-product fraction within the hydrogel (62–70%), demonstrating a promising route for converting them into valuable functional materials. Furthermore, the ability to reload these hydrogels with additional hydrosol or wastewater further enhances their valorisation potential.

3.2.3. Swelling capacity

Swelling is a fundamental property of hydrogels, driven by their ability to absorb water. Fig. 5 illustrates the swelling equilibrium profile of the hydrogels in distilled water at room temperature. All systems reached equilibrium after 48 h, with significant differences in swelling capacity (3383% to 8107%), reflecting their high water-absorption potential. When PECs are submerged in water, the functional groups on their chains dissociate, promoting swelling. This is due to ionisable or protonated functional and hydrophilic groups interacting with water molecules, such as hydroxyl, carboxylate, and quaternary amino groups. Additionally, the relaxation of the polymer chains contributes to the overall swelling behaviour [55,61]. The pH of the solution also affects the swelling behaviour, as it influences the protonation and deprotonation of the functional groups [62]. In the C-based systems (Fig. 5 (A)), FTIR analysis indicated polymer complexation in all systems, but their swelling abilities varied significantly. The Ca and Cb systems showed higher swelling (7786% and 5341% after 48 h, respectively), driven by the pH effect on hydrogel formation, in which the polymeric matrix featured available anionic and cationic groups for water interaction. For example, at lower pH (Ca), ionised amino groups can repel each other, leading to matrix relaxation and enhanced water uptake [63]. Conversely, the neutral system (Cn) had the lowest swelling capacity (3383% after 48 h) due to fewer free ionisable groups. Rao and co-workers [64] studied CH/XG polyelectrolyte hydrogels developed under analogous Cn conditions. After 24 h, their system showed a swelling capacity of about 2750%. Similarly, Ngwabebhoh et al. [65] reported a swelling ratio of approximately 2000% in phosphate-buffered saline solution at 37 °C for the same period. Both values are slightly lower than the 3373% observed in the present Cn system, highlighting its enhanced swelling capacity.

The pH also influenced the swelling behaviour of hydrogels incorporated with the by-product's H and W, affecting both polymer-polymer and polymer-bioactive compound interactions. In this scenario, FTIR analysis revealed the presence of entrapped compounds, which modified the hydrogel's swelling capacity by adjusting the balance between hydrophilic and hydrophobic groups and their molecular interactions [66].

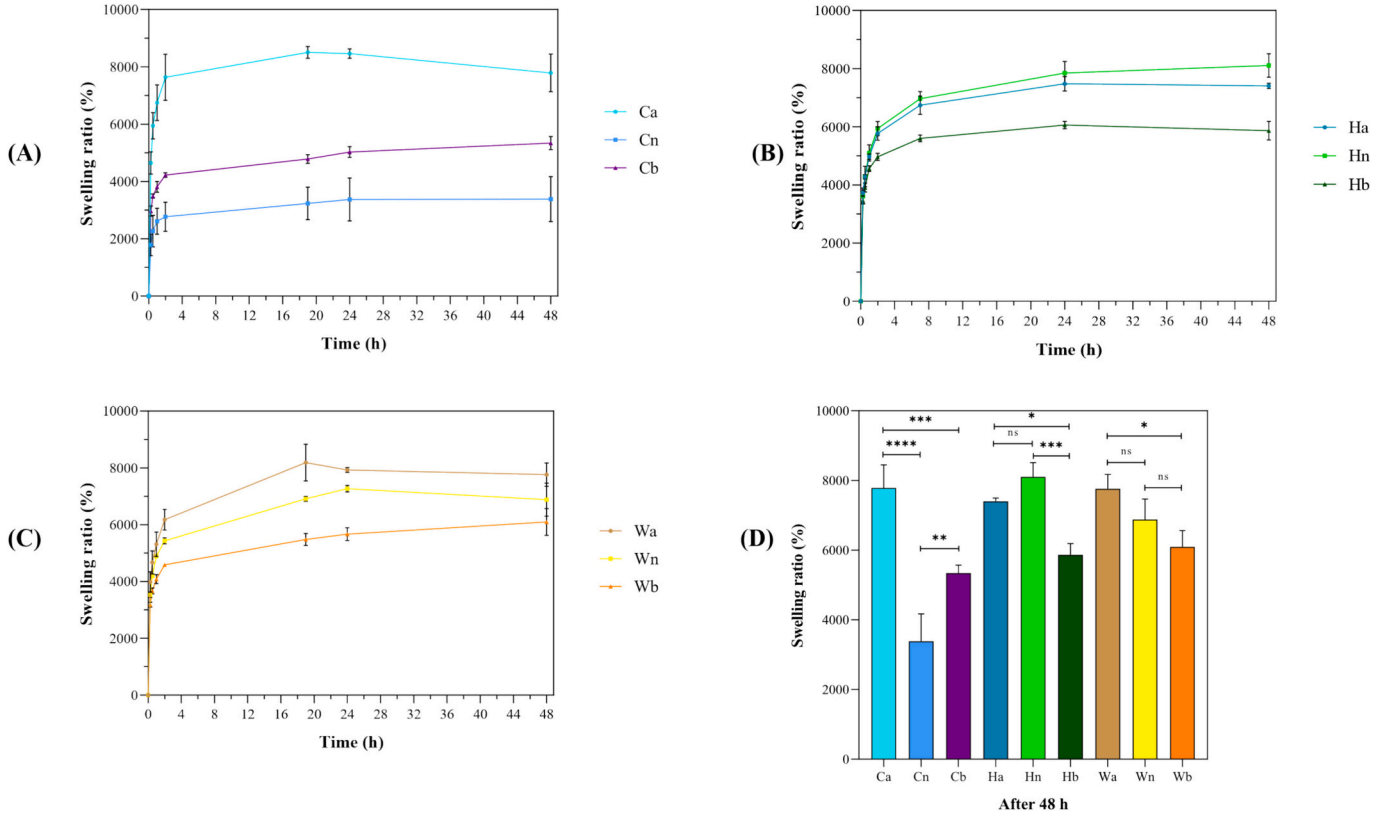

Fig. 5. Swelling ratio for (A) control-based systems, (B) hydrosol-based systems, (C) wastewater-based systems within 48 h in distilled water at room temperature, and (D) statistical comparison between systems at 48 h. Significance levels are indicated as **** ($p < 0.0001$); *** ($p < 0.001$); ** ($p < 0.01$); * ($p < 0.05$), and ns (not significant).

This resulted in different swelling capacities, as shown in the H-based systems (Fig. 5 (B)) and W-based systems (Fig. 5 (C)). After 48 h, the swelling capacities were 7405%, 8107%, and 5868% for Ha, Hn, and Hb, respectively, and 7764%, 6883%, and 6096% for Wa, Wn, and Wb, respectively. Moreover, alongside changes in the hydrogel's internal structure and the availability of free ionisable groups after polymer complexation, water diffusion into the hydrogel causes swelling, releasing the entrapped compounds and opening channels that generate additional hydrogen-bonding sites with water [24,67].

Significant differences in the 48-h swelling ratio across the same base systems at different pH values are evident in Fig. 5 (D). In the C-based systems, Ca exhibited higher swelling than Cn ($p < 0.0001$) and Cb ($p < 0.001$). For H-based systems, Hn differed significantly from Hb ($p < 0.001$). In W-based systems, Wa differed from Wn ($p < 0.01$) and Wb ($p < 0.05$). Multiple comparisons for all systems are provided in the Supplementary Material. Based on the swelling profiles, 3 h was selected as the swelling time, since all hydrogels reached a swelling equilibrium within this period.

The swelling kinetics of all base hydrogel formulations were analysed using the Korsmeyer–Peppas (Table 2). The kinetic constant (k) varied among formulations, with Ca exhibiting the fastest swelling, as indicated by the highest k value. The diffusion exponent (n) was below 0.5 for all systems, confirming diffusion-controlled swelling as the dominant mechanism. High coefficients of determination ($R^2 \geq 0.955$) confirm the model's reliability and the derived kinetic parameters. Swelling is governed by the polymer network, the presence of ionisable groups, interactions with loaded compounds, and the pH of the surrounding medium, making it a critical parameter for drug release, soft actuation, stable implantable devices, wound management, and tissue-regeneration scaffolds [68]. Overall, these results suggest that differences in swelling rate are primarily governed by water diffusivity through the polymer network.

3.2.4. Morphological characterisation

The SEM images of the neutral base hydrogel systems (Cn, Hn and Wn) are presented in Fig. 6. Cross-sectional analysis of fractured, dried hydrogels revealed distinct microstructural changes in each system. Cn exhibited a compact structure with small, distributed pores, while Hn also showed a dense, compact morphology but with almost no pores, suggesting tighter polymer packing and a higher crosslinking degree. In contrast, Wn showed a porous network with interspersed larger voids with regions resembling the Cn and Hn structures, indicating a heterogeneous porosity. These morphological differences, influenced by the polymer packing and the presence of entrapped compounds, correlated well with the observed swelling behaviour and were supported by FTIR results. Similarly, Cheng et al. [69] reported a dense, rough surface in a PEC hydrogel loaded with carvacrol, indicating effective protection of the active compound, comparable to that observed in the Hn system encapsulating citral, also an oxygenated monoterpene. Another study by Barbosa et al. [48] reported a CH/XG polyelectrolyte system that yielded a homogeneous, well-defined surface, comparable to the Cn system.

Summarising, the characterisation of the base hydrogel systems provided insights into the effect of pH on hydrogel formation. This parameter was crucial for understanding the potential interactions within the system, as evidenced by FTIR, H and W entrapment, swelling capacity, and morphological characterisation. Chemical structure analysis confirmed successful polymer complexation and the effective entrapment of H and W within the hydrogel matrix, contributing to enhanced swelling behaviour. These properties are fundamental for the development of functional hydrogel systems.

Table 2
Swelling kinetics of base hydrogel systems.

System	k	n	R^2
Ca	0.861	0.308	0.981
Cn	0.761	0.251	0.955
Cb	0.715	0.169	0.958
Ha	0.641	0.212	0.997
Hn	0.624	0.240	0.998
Hb	0.745	0.191	0.993
Wa	0.636	0.209	0.998
Wn	0.649	0.208	0.988
Wb	0.671	0.172	0.986

Ha, Hn, Hb, Wa, Wn, Wb, and Ca, Cn, Cb denote samples, where H = hydrosol, W = wastewater, C = control, and a, n, b = final pH (acidic 4, neutral 7, basic 11). Swelling parameters fitted to Korsmeyer-Peppas (KP) model. The table includes kinetic parameters (k, n, and R^2). Data highlight differences in swelling behaviour among formulations.

3.3. Hydrogels reload step

The base hydrogels (C-, H-, and W-based) were reloaded with the H and W by-products to increase performance. Upon contact with each by-product, the hydrogels swell, creating channels that expose additional binding sites, favouring polymer-bioactive compound interactions and allowing more components to be entrapped into the polymeric matrix [70,71]. The reloading capacity of the C- and H-based systems is shown in Table 3. In this assay, H and W were used directly in their naturally acidic forms. The reload effect can be observed in acidic systems (Ca and Ha), where the CH-protonated amino groups strengthen their electrostatic interactions with anionic molecules, thereby enhancing the overall loading capacity [46]. Neutral systems (Cn and Hn) demonstrated lower reloading capacities due to the limited availability of functional groups for extra binding sites, resulting from strong interactions and chain entanglement between polymers and H bioactive compounds. Conversely, in alkaline systems (Cb and Hb), the carboxyl groups become more accessible, facilitating electrostatic interactions with cationic molecules [72]. Excluding the Cn system, which exhibited the lowest loading capacity, the higher compatibility of hydrogels with H compared to W resulted in higher reloading capacities. This step not only enhanced the incorporation of bioactive compounds into the hydrogel matrix but also opened a second sustainable route for the valorisation of otherwise discarded by-products.

3.3.1. Release studies

The release profiles of H and W from selected hydrogel systems were investigated in distilled water at 25 °C, to confirm the successful incorporation and elucidate their release mechanisms. Neutral loaded systems (Hn and Wn) and reloaded systems (Hn + H and Wn + H) were evaluated and values expressed per gram of dried hydrogel (Fig. 7). Considering the hydrosol release profiles (Fig. 7 (A)), the reloaded systems showed the highest cumulative release after 24 h, reaching 17,908 mg/g for Hn + H and 20,554 mg/g for Wn + H, while the loaded system, Hn, released 5795 mg/g. For the W systems (Fig. 7(B)), Wn and Wn + H showed similar cumulative release profiles, reaching values of 31,446 and 42,154 mg/g, respectively.

Hydrogel release rates depend on network morphology, ranging from faster to slower release patterns as the structure densifies [73,74]. This behaviour was evident in the results, as Hn exhibited the lowest H release, aligning with its dense, highly crosslinked network observed by SEM, which restricted diffusion. In contrast, reloaded systems (Hn + H and Wn + H) showed significantly higher release, as the reloading process involved hydrosol interactions with surface-accessible polymer groups or swelling-induced channels, allowing an easier diffusion. Wn and Wn + H released similar amounts of W-derived bioactives, reflecting weaker polymer–phenolic interactions and a highly porous, heterogeneous morphology, as corroborated by SEM. Furthermore, FTIR spectra of the reloaded systems confirmed the incorporation of bioactive components, presenting characteristic peaks, complementing the findings from the loading and release analyses. Overall, these results indicated that both chemical cross-linking and network porosity governed the release kinetics, while reloading increased release capacity by

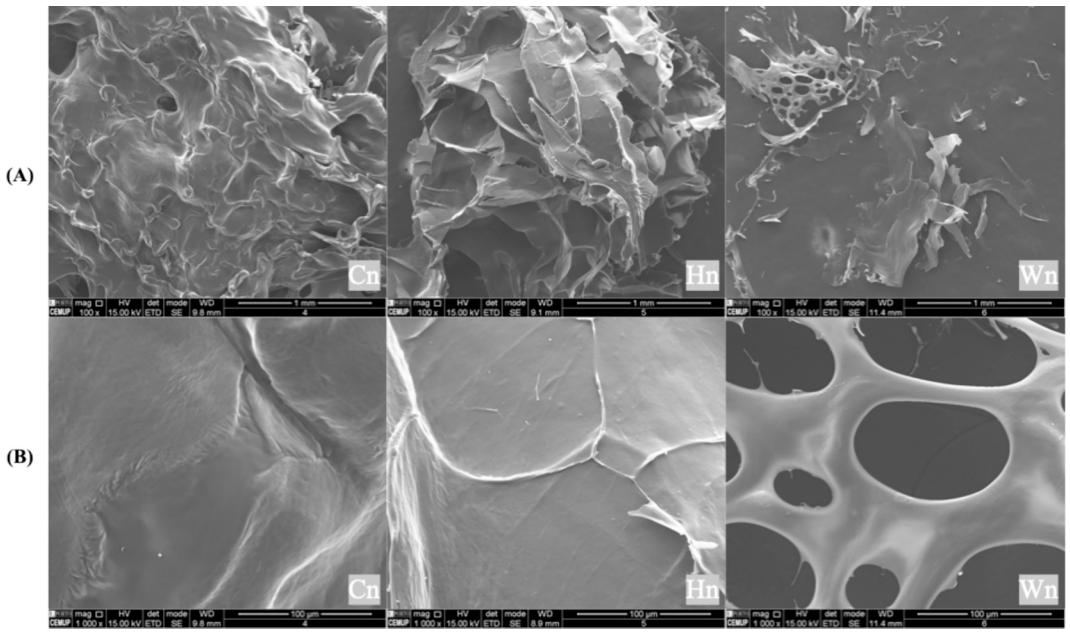

Fig. 6. SEM images of Cn, Hn and Wn systems observed at (A) 100× and (B) 1000×.

Table 3
Base hydrogel systems reloading capacity (RC%) with hydrosol and wastewater.

Reloading with H	RC (%)	Reloading with W	RC (%)
Ca + H	42.0 ± 0.65^{c}	Ca + W	34.1 ± 0.70^{cde}
Cn + H	19.2 ± 0.67^{ab}	Cn + W	16.8 ± 0.80^{a}
Cb + H	31.3 ± 2.07^{de}	Cb + W	27.1 ± 2.61^{be}
Ha + H	41.2 ± 0.10^{c}	Ha + W	36.0 ± 1.51^{cde}
Hn + H	31.9 ± 1.59^{de}	Hn + W	27.2 ± 1.35^{be}
Hb + H	35.5 ± 5.33^{cde}	Hb + W	36.2 ± 7.93^{cd}

Ha, Hn, Hb, and Ca, Cn, Cb denote samples, where H = hydrosol, W = wastewater, C = control, and a, n, b = final pH (acidic 4, neutral 7, basic 11). '+H' and '+W' indicate reloading. Values are presented as Mean ± SD. Different letters indicate statistically significant differences between groups (Tukey's HSD, $p < 0.05$). Groups sharing at least one letter are not significantly different.

modifying the hydrogels' structure and by increasing the amount of loaded compounds, which could be promising for improving the hydrogels' bioactivity.

Release kinetics were analysed using pseudo-first order, Higuchi, and Korsmeyer-Peppas (KP) models (Table 4). These models aimed to elucidate the mechanisms of release of active compounds from polymeric systems. First-order release kinetics depend on the amount of compounds remaining in the matrix; the Higuchi model describes Fickian diffusion–controlled release, and the Korsmeyer–Peppas model characterises the release profile by identifying the dominant transport mechanism. Pseudo-first-order and Korsmeyer-Peppas models describe the kinetics effectively, whereas the Higuchi model captures only part of the diffusion process, corresponding to the initial diffusion-controlled stage of release [75]. Among the systems, Wn and Wn + H exhibited higher release rate constants, indicating faster release than hydrosol-based formulations. The KP diffusion exponent ($n \leq 0.45$) for all samples indicated Fickian diffusion as the dominant release mechanism, with Wn + H showing borderline anomalous behaviour. The relatively high coefficients of determination (R^2 up to 0.93) indicate an adequate model fit. Overall, the KP model provided the most suitable fit for most systems (R^2 = 0.84–0.93), except for Hn, which fitted better with the Higuchi model (R^2 = 0.84), as shown in Fig. 8. Most hydrogels, therefore, exhibited diffusion-controlled release from the polymer matrix. Reloaded hydrogels (Hn + H and Wn + H) showed faster and higher cumulative release than the loaded systems, demonstrating enhanced delivery of bioactives. These results aligned with the swelling and SEM

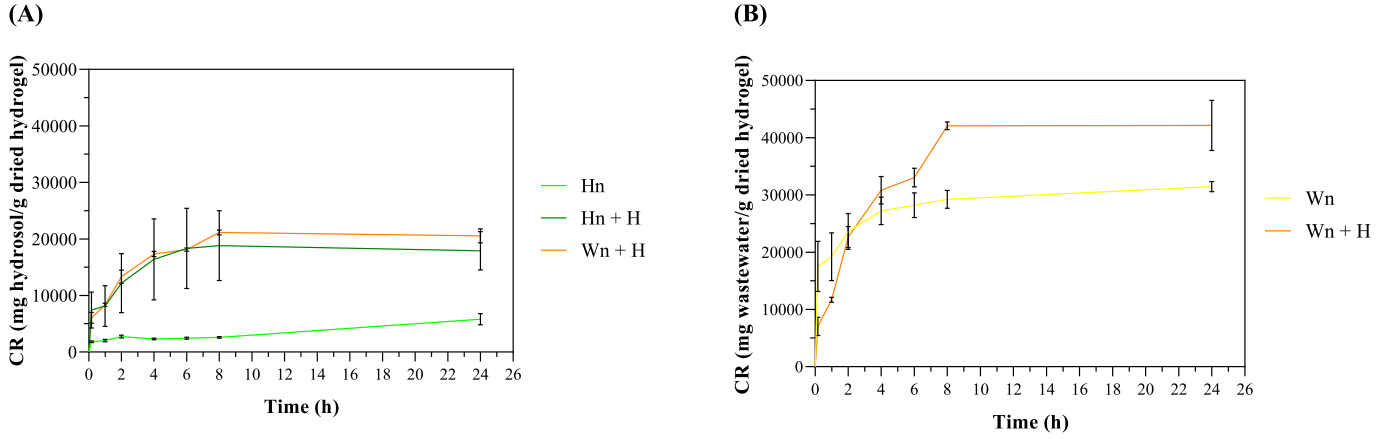

Fig. 7. Release profiles of H and W from loaded and reloaded neutral base systems. (A) Hydrosol release (mg/g dried hydrogel) measured at 243 nm; (B) Wastewater release (mg/g dried hydrogel) measured at 328 nm.

Table 4
Release kinetics and transport mechanisms of loaded and H-reloaded hydrogel systems.

System	PFO k_1	R^2	Higuchi k_H	R^2	KP k	n	R^2	Transport mechanism
Hn	0.000723	0.391	121.266	0.840	0.173	0.186	0.627	Fickian diffusion
Hn + H	0.001838	0.455	462.475	0.685	0.222	0.225	0.835	Fickian diffusion
Wn + H (H release)	0.002256	0.870	549.640	0.759	0.149	0.286	0.909	Fickian diffusion
Wn	0.004743	0.891	675.232	0.646	0.396	0.133	0.932	Fickian diffusion
Wn + H (W release)	0.010301	0.751	1207.538	0.828	0.066	0.408	0.926	Fickian/borderline anomalous

Hn and Wn denote samples, where H = hydrosol, W = wastewater, and n = final pH (neutral 7). '+H' indicate reloading. Release parameters fitted to pseudo-first order (PFO), Higuchi, and Korsmeyer-Peppas (KP) models for hydrosol- and wastewater-based hydrogels. The table includes model constants, exponent n, goodness of fit (R^2), and inferred transport mechanism.

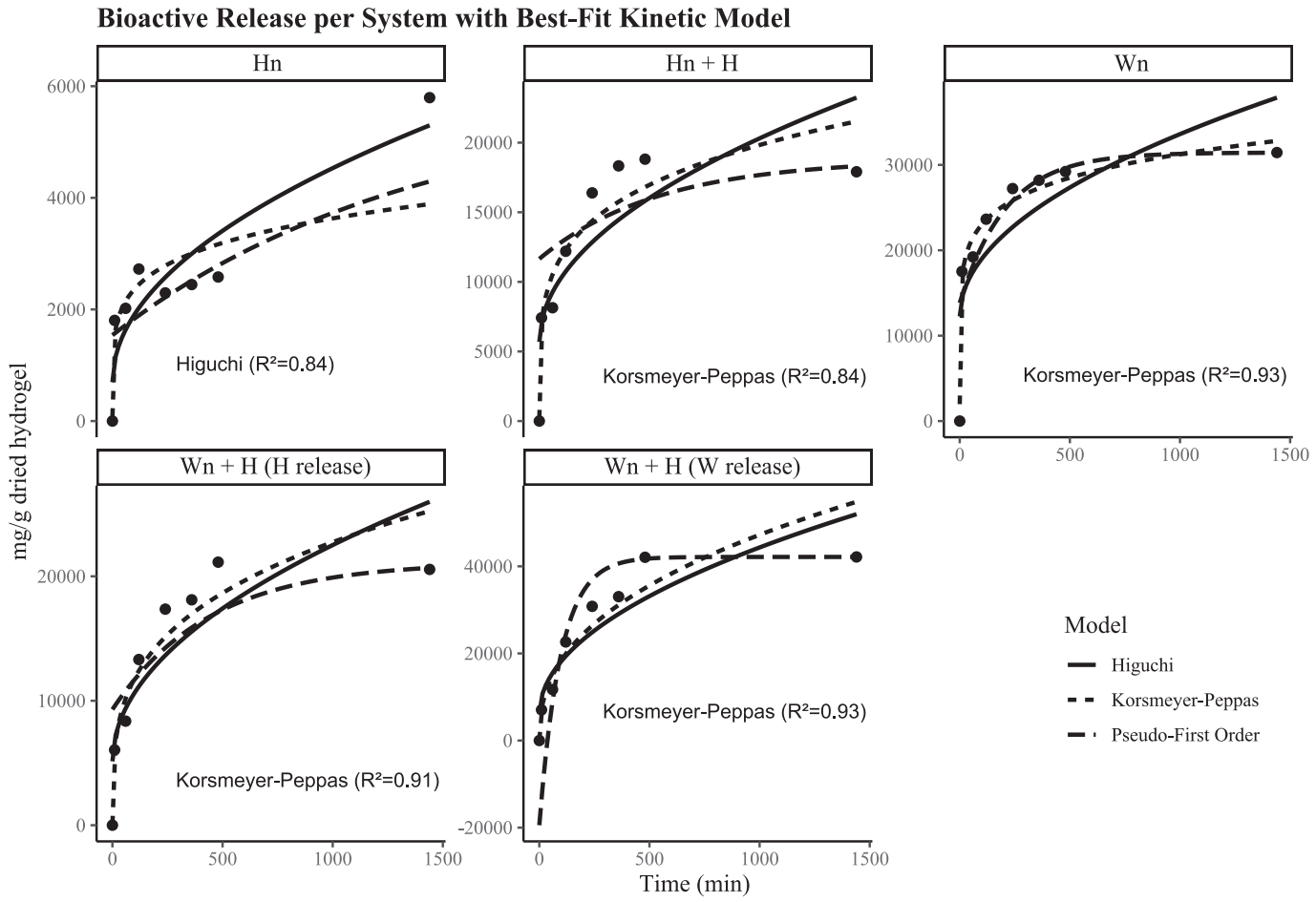

Fig. 8. Hydrosol and wastewater release from hydrogel systems with best-fit kinetic model generated by RStudio (4.3.0).

results, highlighting the combined influence of the network structure, polymer–bioactive interactions, and swelling behaviour.

3.3.2. *Rheological characterisation*

The rheological behaviour of the neutral base hydrogels (Cn, Hn, and Wn) and two reloaded systems (Hn + H and Wn + H) was evaluated through flow, amplitude, and frequency sweep tests at 25 °C, as shown in Fig. 9. Flow curves (Fig. 9 (A)) revealed shear-thinning behaviour for all systems, as evidenced by a decrease in viscosity with increasing shear rate, in line with previous studies on polysaccharide-based hydrogels, including CH-XG systems [29,34,76,77]. This response relates to the structural deformation of the entangled polymer network, in which higher shear rates elongate the chains, aligning them in the flow direction [78,79]. In this context, the viscosity of each system depends on polymer-polymer and polymer-bioactive compound interactions, which sometimes result in higher viscosities for the H- and W-based systems compared to the C-based and H-reloaded systems. Studies examining samples incorporating natural compounds reported similar shear-thinning behaviour [78,80–82].

Amplitude sweeps assay (Fig. 9 (B)) enables the determination of the linear viscoelastic region (LVR) and the critical strain at the elastic–viscous transition, reflecting the changes in storage modulus (G′) and loss modulus (G″). The LVR indicates the region where the moduli (G′ and G″) are independent of the applied deformation [81]. At low strain, all systems presented elastic gel behaviour (G′ > G″). The G′ at 0.01% strain was 975.6, 1544.5, 1126.2, 329.7, and 142.6 Pa for Cn, Hn, Wn, Hn + H, and Wn + H, respectively. As the shear strain increased, G′ remained independent of strain until reaching the critical point, beyond which it decreased considerably. Simultaneously, G″ increased, indicating a shift to a viscous behaviour (G″ > G′) associated with the structure breakdown due to the applied deformation [46]. The critical strain values (G′ = G″), corresponding to the elastic-viscous transition

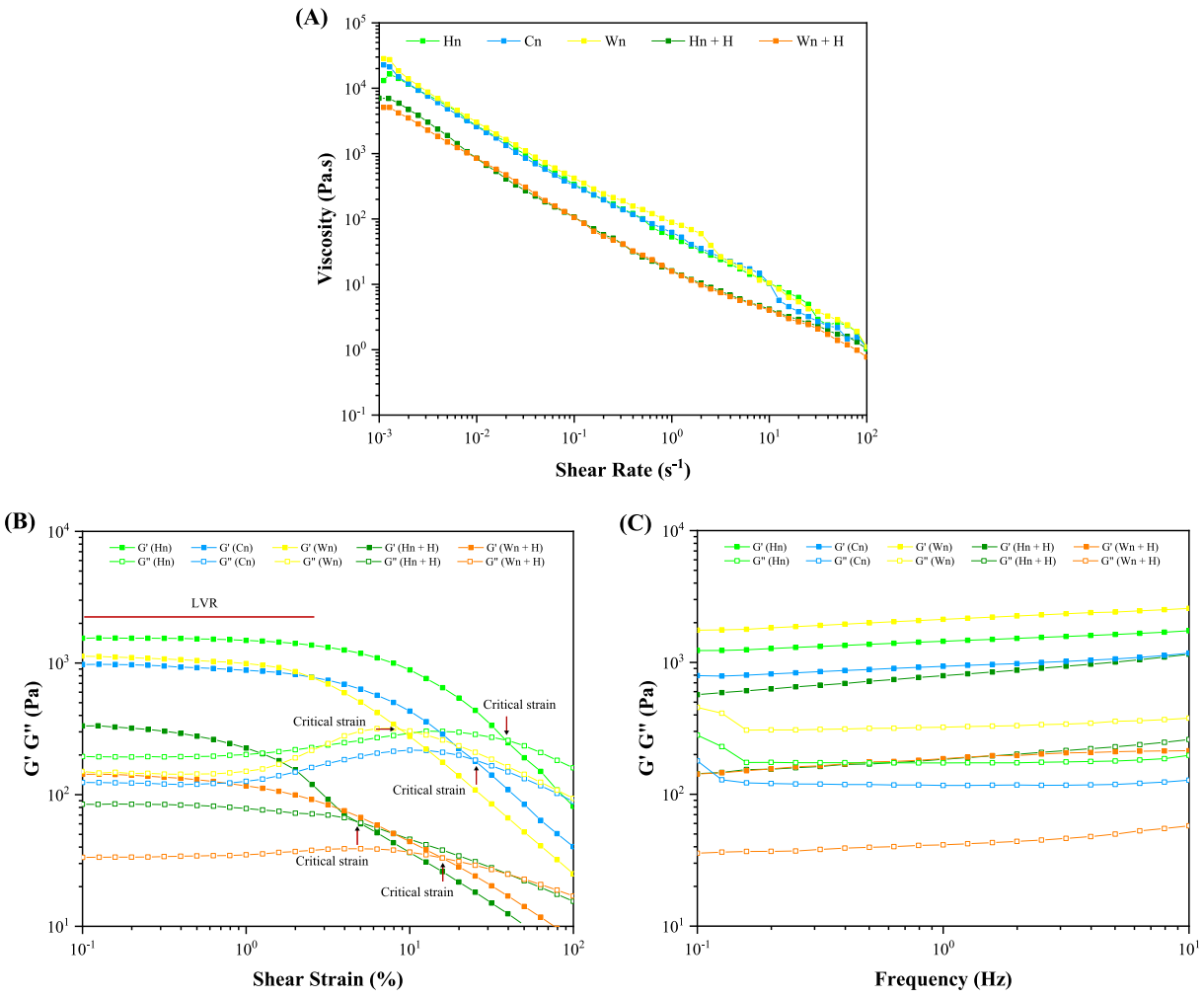

Fig. 9. Rheological properties of the neutral hydrogel systems (Cn, Hn, and Wn) and reloaded neutral systems (Hn + H, and Wn + H) at 25 °C, including (A) flow curves, (B) amplitude sweep tests and (C) frequency sweep tests.

point, varied among the loaded systems. Hn system showed the highest critical strain (40.0%), indicating the most stable network, possibly due to stronger polymer-citral interactions (present in the H), which enhanced resistance to the gel-to-fluid transition, followed by Cn (25.2%) and Wn (8.0%). Evaluation of the reloading step revealed distinct rheological responses compared to the initially loaded systems. In particular, Wn + H showed a higher critical strain (15.9%) than Wn system, indicating increased resistance to deformation, which may be attributed to further interactions between citral and previously available active sites within the polymer matrix. In contrast, the Hn + H system exhibited a lower critical strain (5.0%), suggesting increased susceptibility to structural breakdown under low deformation, likely due to reduced availability of active sites and weaker interactions following the reloading step. The additional bioactive incorporation through the swelling-diffusion reloading process appeared to partially relax the original polymer-polymer network. These findings highlighted that network stability depends on polymer-bioactive interactions, with Hn exhibiting the strongest elastic properties, which correlate with a denser, more compact microstructure, as observed by SEM.

For all hydrogels, the frequency sweep tests conducted within the LVR (Fig. 9 (C)) confirmed a predominant elastic behaviour ($G' > G''$) across all frequencies, highlighting the hydrogel's dominant solid-like, elastic nature and indicating retention of the network structure under the applied deformation. Additionally, the results provided valuable insights into the internal structures of the hydrogels in the LVR, including the loading and reloading effect. The systems loaded with EO by-products showed higher G' values than the control system, suggesting network reinforcement through additional polymer-bioactive interactions, such as hydrogen bonding, hydrophobic associations, and π–π stacking, thereby influencing the hydrogels' viscoelastic properties [80,83–85].

The reloaded systems showed lower G' values across all systems, reflecting reduced crosslinking density and increased polymer chain mobility. These results indicated that the initial loading step strengthens the hydrogel matrix, while the reloading can soften the network.

Overall, the developed systems in this study presented promising rheological properties, including a shear-thinning behaviour and dominant elasticity ($G' > G''$), indicative of a primarily solid-like structure. This network structure is advantageous for applications requiring structural integrity, such as wound dressings, topical formulations, and food packaging materials [64,86–88]. Additionally, the softer, shear-responsive characteristics of these systems may be beneficial for applications demanding enhanced spreadability or injectability [89,90]. In the study of Cui et al. [91], a hydrogel system loaded with *Satureja montana* essential oil exhibited $G' > G''$ across the entire analysed frequency range, confirming its predominantly elastic behaviour. The incorporation of essential oil resulted in a denser gel network and increased hardness compared to the control (without EO), suggesting its potential as a carrier for volatile antibacterial agents in food packaging applications to extend product shelf life. Similarly, Chen et al. [23] incorporated thyme oil into hydrogel matrices and observed that its inclusion increased the network density, an effect confirmed by SEM

analysis. Their findings further supported the suitability of such enriched hydrogels as packaging materials. Another study by Suflet et al. [92] examined chitosan/pullulan hydrogels loaded with clove oil and found that the oil-loaded hydrogels exhibited improved mechanical properties and rapid shape recovery, indicating their potential as promising wound-dressing materials. These results highlight the versatility of hydrogel systems, in which rheological properties can be tailored through controlled loading of bioactives to meet desired properties and application requirements.

3.4. Antioxidant activity: ABTS and DPPH assays

The antioxidant potential of all hydrogel systems, assessed via DPPH and ABTS assays, is shown in Fig. 10. The results corroborated the reload step's positive effect when analysing the C-based systems (Fig. 10 (A)). The unloaded systems (Ca, Cn, and Cb) did not demonstrate antioxidant activity; however, a noticeable effect was observed following the reload step, which enhanced the bioactivity due to the entrapped bioactive compounds. Similar behaviour was observed in the H- and W-based systems (Fig. 10 (B) and (C)), with higher antioxidant potential after reloading. Overall, hydrogels loaded and reloaded with wastewater exhibited the highest antioxidant capacity, consistent with the high phenolic content of the wastewater by-product, known to efficiently neutralise free radicals and reactive oxygen species [13,93–96].

These findings corroborated the release behaviour, confirming that the hydrogel systems can effectively incorporate and release bioactive compounds by diffusion through the polymer matrix. The reloading step increased the bioactive concentration, reflected in an enhanced antioxidant potential. This high bioactivity observed in H- and W-based systems can be attributed to their phenolic content, as shown in Table 5. For example, the neutral system Wn increased phenolics from 1.27 to 2.37 after reloading (Wn + W). Among all systems, the H-based systems reloaded with W (Ha + W, Hn + W, Hb + W) showed the highest scavenging capacity (85–91% for ABTS and 59–70% for DPPH) and phenolic/flavonoid content (3.77–6.04 mg/g for phenolics and 3.39–5.29 mg/g for flavonoids), highlighting the advantage of combining and valorising EO by-products to develop antioxidant hydrogel systems. Significant differences between the systems were observed, highlighting the influence of pH on the bioactivity, in agreement with the hydrogel characterisation results. Multiple comparisons for all systems are provided in the Supplementary Material.

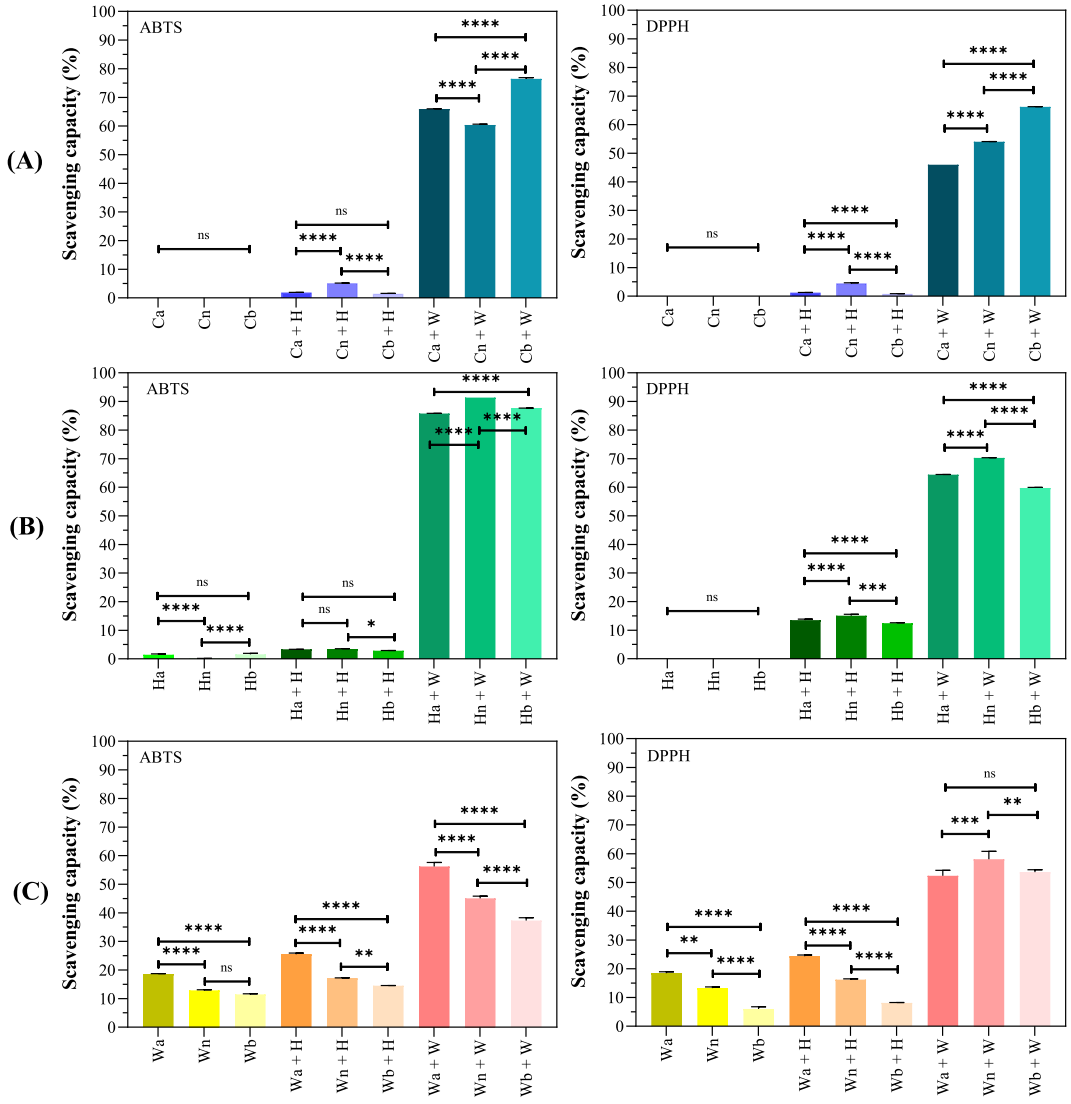

Fig. 10. Antioxidant activity of all developed hydrogel systems (unloaded, loaded and reloaded), namely (A) control-based systems, (B) hydrosol-based systems, and (C) wastewater-based systems, assessed by their ability to scavenge free radicals ABTS and DPPH. Significance levels are indicated as **** ($p < 0.0001$); *** ($p < 0.001$); ** ($p < 0.01$); * ($p < 0.05$), and ns (not significant).

Table 5
Total phenolic and flavonoid content of hydrogel systems after reloading with *A. citrodora* EO by-products.

Hydrogel systems	Phenolic content (mg gallic acid equivalent/g dried hydrogel)	Flavonoid content (mg catechin equivalent/g dried hydrogel)
Wa	0.73 ± 0.02^{f}	0.04 ± 0.01^{f}
Wn	1.27 ± 0.03^{e}	0.58 ± 0.11^{e}
Wb	0.21 ± 0.03^{g}	0.02 ± 0.11^{f}
Wa + W	2.76 ± 0.03^{c}	2.75 ± 0.07^{c}
Wn + W	2.37 ± 0.09^{d}	1.95 ± 0.13^{d}
Wb + W	2.88 ± 0.16^{c}	2.51 ± 0.04^{c}
Ha + W	6.04 ± 0.13^{a}	5.29 ± 0.08^{a}
Hn + W	3.93 ± 0.11^{b}	3.47 ± 0.32^{b}
Hb + W	3.77 ± 0.10^{b}	3.39 ± 0.07^{b}

Ha, Hn, Hb, and Wa, Wn, Wb, denote samples, where H = hydrosol, W = wastewater, and a, n, b = final pH (acidic 4, neutral 7, basic 11). '+W' indicate reloading. Values are expressed as mean ± SD ($n = 3$). Different superscript letters indicate significant differences among groups within each dataset (phenolics or flavonoids) according to one-way ANOVA followed by Tukey's HSD test ($p < 0.05$).

3.5. Antimicrobial activity

The adapted method under dynamic contact conditions was used to evaluate the antimicrobial effectiveness of the neutral systems against planktonic microbial cultures (*S. aureus* and *E. coli*), as shown in Figs. 11 and 12. Statistical analysis was used to identify significant differences between selected samples (Cn, Hn, Wn, Hn + H, and Wn + H) to determine whether the bioactive compounds from EO distillation by-products can contribute to microbial reduction. The impact of each hydrogel system on bacterial activity over time was compared with that of a control group (without hydrogel). It is known that CH possesses inherent antimicrobial properties due to electrostatic interactions that damage cell structures, increase membrane permeability, or form an impermeable layer on pathogens, blocking nutrient uptake and altering metabolite excretion [97,98]. The microbial reduction of the unloaded system (Cn) against both microorganisms corroborated this inherent characteristic associated with CH.

The samples reduced the *S. aureus* bacterial activity from the initial time (t_0), being stronger over time (Fig. 11 (A)). Statistical multiple-comparison analysis confirmed significant time-dependent differences among systems at each studied interval (Fig. 11 (B)). The most effective system was the Hn + H reloaded hydrogel, which exhibited a bactericidal impact resulting in 100% bacterial reduction after 8 h. After 1 h, its potential was significantly greater than that of all other systems ($p < 0.0001$). The Hn resulted in the second-most effective system, achieving a significant 3-log reduction in CFU count after 8 h compared with the control ($p < 0.0001$). These results emphasised the significance of bioactive compounds in EO by-products, particularly hydrosol, entrapped within the hydrogel structure, providing antibacterial activity, as demonstrated by comparison with the unloaded system (Cn). The Hn system showed a significant difference ($p < 0.0001$) after 0.5 h, while the Hn + H system proved to be effective from the initial contact (t0) ($p < 0.001$). Furthermore, these findings highlighted the benefits of the reloading step, where the increased H concentration enhanced the system's antimicrobial effectiveness. In contrast, the Wn and Wn + H (systems holding W) showed no significant differences from the unloaded system (Cn), suggesting that their antimicrobial potential may be attributed only to the chitosan. W's lower entrapment and antimicrobial activity could explain this outcome. The antimicrobial activity of the studied systems against *E. coli* (Fig. 12(A)) also showed enhanced antimicrobial activity over time, with statistically significant differences (Fig. 12(B)). However, *E. coli* showed greater resistance than *S. aureus*, resulting in lower microbial reduction after 8 h. Between 0.5 and 4 h, the Hn showed the highest microbial reduction, achieving a significant 1-log reduction in CFU count compared to the control ($p < 0.0001$). At the end of the assay (8 h), the most effective system, Hn + H, achieved a 2-log reduction in CFU count compared to the control ($p < 0.0001$). These findings also supported the effectiveness of H bioactive compounds in hydrogel systems, an effect not observed with the W-loaded systems. Although phenolic compounds can exhibit antimicrobial activity, their effectiveness depends on molecular interactions, bioavailability, and the surrounding matrix [99]. At neutral pH, weaker interactions reduce entrapment and bioactivity. Morphological analysis showed that W-based systems have a porous, heterogeneous structure, leaving phenolics exposed on surface-accessible polymer groups, thereby rendering them less effective. Even after reloading with H, the antimicrobial activity remained limited, likely due to insufficient retention and availability, as well as bacterial cell structure, compound concentration, and exposure time [23]. These results indicated that polymer–phenolic interactions in W-systems preserved antioxidant capacity but restricted antimicrobial efficacy.

The hydrogel systems generally demonstrated greater antimicrobial activity against Gram-positive bacteria, which may be related to differences in the structural features of their cell walls, compared to Gram-negative bacteria. Gram-negative bacteria have a double membrane structure, with the outer membrane containing lipopolysaccharides. In contrast, Gram-positive bacteria have a single membrane with a thicker peptidoglycan layer in their cell wall [100]. Ma et al. [101] investigated a chitosan/carboxymethyl cellulose hydrogel system loaded with citral, the main bioactive compound in the hydrosol of this study. Their results showed more potent antibacterial activity against Gram-positive bacteria than against Gram-negative bacteria, particularly against *S. aureus*, followed by *E. coli*. These findings aligned with our results, as the similar loaded-hydrogel system showed comparable antibacterial effects. Particularly, citral has been recognised to show high levels of reactive oxygen species in cells, induce morphological changes, disrupt cell membrane fluidity and permeability, and compromise membrane integrity, leading to dysfunction, leakage of intracellular macromolecules, and rapid cell death [102]. Hydrosols containing citral isomers as their primary compounds have been reported to exhibit antimicrobial activity [103,104]. Additionally, hydrogel systems incorporating essential oil bioactives, being released via diffusion (as observed in release profile modelling results), exhibited antimicrobial activity against *S. aureus* and *E. coli*, highlighting their potential for intelligent food packaging applications to extend shelf life and prevent microbial contamination [23,69]. Another study, conducted by Stoleru et al. [105], evaluated chitosan-based hydrogels loaded with essential oils, which markedly enhanced antimicrobial activity compared with unloaded counterparts. The hydrogels (freshly prepared) were more effective against *S. aureus* than *E. coli*, initially inhibiting 74% of *S. aureus* growth and retaining 51% of inhibition after six months of shelf storage. This sustained activity indicated a successful EO embedding and highlighted the potential of these systems for wound dressings and food-packaging applications.

All hydrogel systems in this work demonstrated significant antimicrobial efficacy over the longer test time (8 h), reducing microbial cultures by more than 96%. The antimicrobial effectiveness of H-systems (loaded and reloaded) correlated with the release assays, as increased diffusion of the hydrosol bioactives, namely citral to exert its effect. These systems successfully concentrated bioactive compounds from a diluted mixture obtained as a by-product (i.e., avoiding the need for additional concentration steps during the obtention of H and W by-products), demonstrating a more efficient direct use of the active components. Overall, these findings highlighted the combined effect of chitosan's inherent antimicrobial potential and citral isomers, effectively targeting cellular changes and disruptions, showing the hydrogel systems' potential as natural antimicrobial agents.

4. Conclusions

This work demonstrated that electrostatically cross-linked

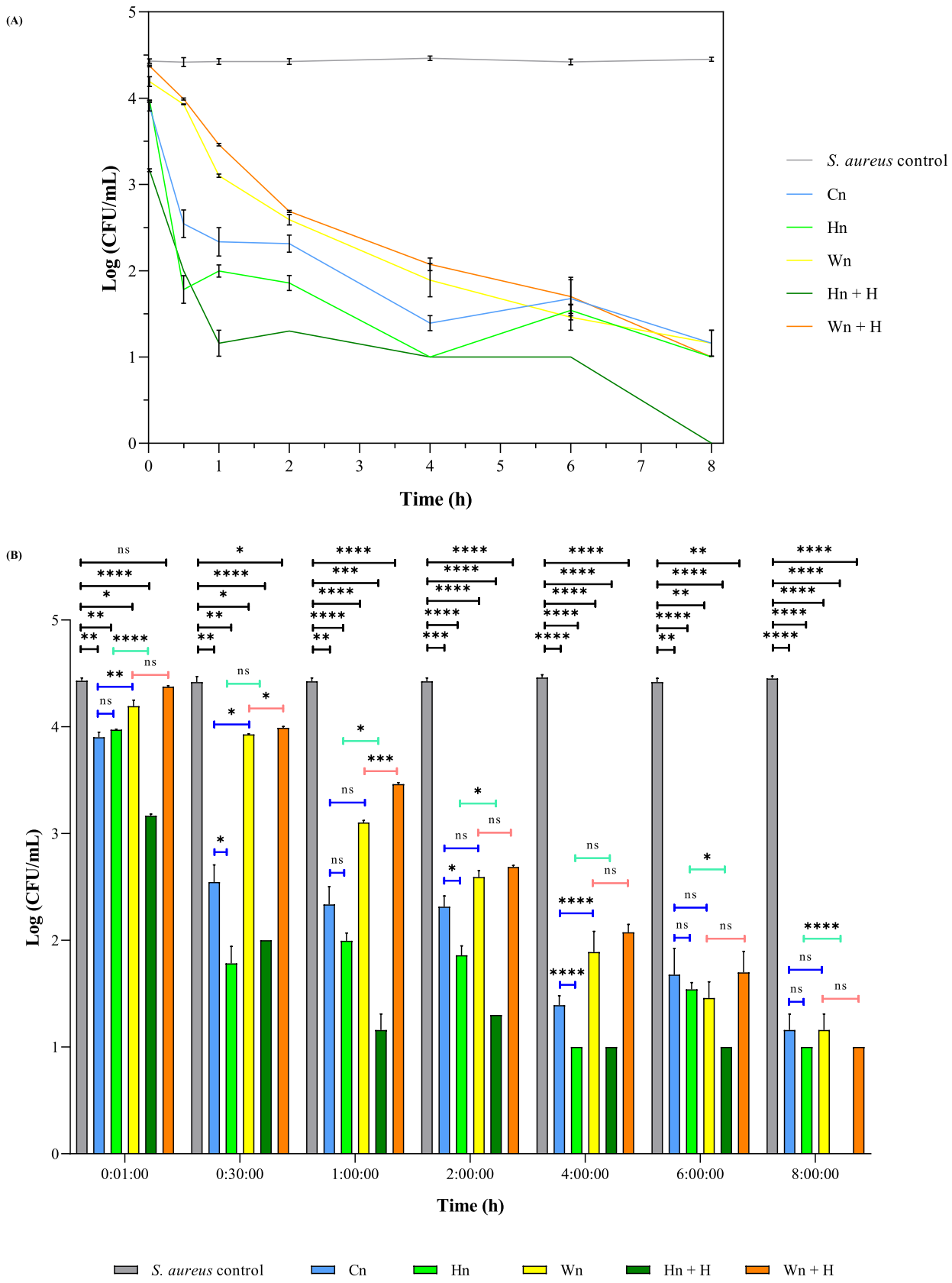

Fig. 11. (A) Quantification of *S. aureus* reduction (Log (CFU/mL)) and (B) Statistical multiple-comparison analysis over time using hydrogel systems and the dynamic contact test method. Significance levels are indicated as **** ($p < 0.0001$); *** ($p < 0.001$); ** ($p < 0.01$); * ($p < 0.05$), and ns (not significant).

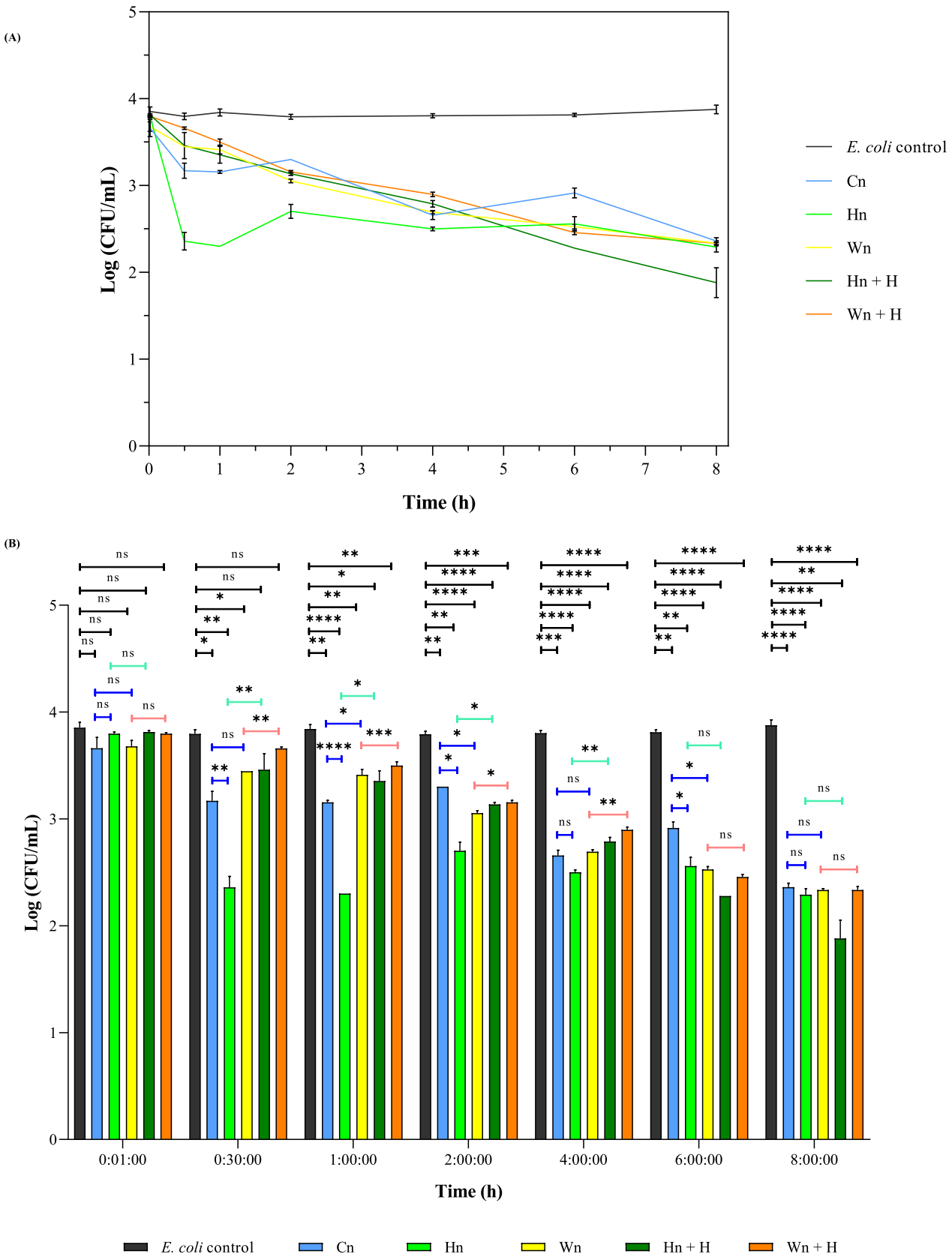

Fig. 12. (A) Quantification of *E. coli* reduction (Log (CFU/mL)) and (B) Statistical multiple-comparison analysis over time using hydrogel systems and the dynamic contact test method. Significance levels are indicated as **** ($p < 0.0001$); *** ($p < 0.001$); ** ($p < 0.01$); * ($p < 0.05$), and ns (not significant).

chitosan–xanthan gum hydrogels successfully entrapped bioactive compounds from *A. citrodora* distillation by-products, with H-based systems (Hn) exhibiting the highest entrapment efficiency (70.3%), and structural integrity. pH and reloading strategies have been shown to modulate hydrogel network density, porosity, and polymer-polymer and polymer–bioactives interactions, directly influencing swelling, release kinetics, antioxidant capacity, and antimicrobial efficacy. All systems (C-, H-, and W-based) exhibited high swelling capacities (3383–8107%), while rheological analysis confirmed shear-thinning behaviour and a dominant solid-like, elastic hydrogel nature.

The reloading approach effectively concentrated highly diluted bioactive compounds from hydrosol and wastewater by-products, thereby enhancing both radical-scavenging activity and microbial inhibition. Reloading with W further boosted antioxidant activity, while H reloading increased antimicrobial capacity. H-based systems (Hn and Hn + H) exhibited effective antimicrobial action against *S. aureus* and *E. coli* within 30 min, outperforming the control system (Cn). These findings emphasised the improved bioactivity achievable from EO by-products (through their direct use) and the clear advantages of reloading to maximise hydrogel functionality.

In conclusion, the CH-XG polyelectrolyte hydrogels integrating green bioactive compounds represent a sustainable, value-added platform for waste valorisation, combining significant antioxidant and antimicrobial potential. Looking ahead, the most promising systems should be assessed for biofilm inhibition and longer-term antimicrobial performance, alongside further optimisation of W-based formulations and exploration of synergistic combinations of both by-products. Their versatile properties make them highly suitable for applications in food packaging, wound dressings, and eco-friendly antimicrobial systems.

CRediT authorship contribution statement

Heloísa H.S. Almeida: Writing – original draft, Methodology, Investigation, Conceptualization. **Arantzazu Santamaria-Echart:** Writing – review & editing, Methodology, Formal analysis. **Joana S. Amaral:** Methodology. **Leandro L. Aquino:** Investigation. **Alírio E. Rodrigues:** Writing – review & editing, Supervision. **Maria-Filomena Barreiro:** Writing – review & editing, Supervision, Resources, Conceptualization.

Declaration of competing interest

The authors declare no conflict of interest.

Acknowledgements

Financial support through national funds FCT/MCTES (PIDDAC): CIMO, UID/00690/2025 (DOI: 10.54499/UID/00690/2025) and UID/PRR/00690/2025 (DOI: 10.54499/UID/PRR/00690/2025); SusTEC, LA/P/0007/2020 (DOI: 10.54499/LA/P/0007/2020); LSRE-LCM, UID/50020/2025 (DOI: 10.54499/UID/50020/2025); and ALiCE, LA/P/0045/2020 (DOI: 10.54499/LA/P/0045/2020). National funding by FCT, Foundation for Science and Technology, through the institutional program contract for scientific employment of A. Santamaria-Echart, and the PhD grant of Heloísa Helena Scorsato de Almeida (DOI: 10.54499/SFRH/BD/148124/2019). Deifil Technology Lda (www.deifil.pt) for supplying the studied plants.

Appendix A. Supplementary data

Supplementary data to this article can be found online at https://doi.org/10.1016/j.ijbiomac.2026.150368.

Data availability

Data will be made available on request.

References

[1] M.A. Abushaheen, A.J. Muzaheed, M. Fatani, W. Alosaimi, M. Mansy, S. George, S. Acharya, D.D. Rathod, C. Divakar, S. Jhugroo, A.A. Vellappally, J. Khan, P. Jhugroo Shaik, Antimicrobial resistance, mechanisms and its clinical significance, Disease-a-Month 66 (2020), https://doi.org/10.1016/j.disamonth.2020.100971.
[2] D.H. Hanna, G.R. Saad, Encapsulation of ciprofloxacin within modified xanthan gum-chitosan based hydrogel for drug delivery, Bioorg. Chem. 84 (2019) 115–124, https://doi.org/10.1016/j.bioorg.2018.11.036.
[3] A. Martínez, M. Manrique-Moreno, M.C. Klaiss-Luna, E. Stashenko, G. Zafra, C. Ortiz, Effect of essential oils on growth inhibition, biofilm formation and membrane integrity of escherichia coli and staphylococcus aureus, Antibiotics 10 (2021), https://doi.org/10.3390/antibiotics10121474.
[4] F. Hong, P. Qiu, Y. Wang, P. Ren, J. Liu, J. Zhao, D. Gou, Chitosan-based hydrogels: from preparation to applications, a review, Food Chem. X 21 (2024), https://doi.org/10.1016/j.fochx.2023.101095.
[5] D. Wu, L. Zhu, Y. Li, X. Zhang, S. Xu, G. Yang, T. Delair, Chitosan-based colloidal polyelectrolyte complexes for drug delivery: a review, Carbohydr. Polym. 238 (2020), https://doi.org/10.1016/j.carbpol.2020.116126.
[6] Y. Zhang, L. Dong, L. Liu, Z. Wu, D. Pan, L. Liu, Recent advances of stimuli-responsive polysaccharide hydrogels in delivery systems: a review, J. Agric. Food Chem. 70 (2022) 6300–6316, https://doi.org/10.1021/acs.jafc.2c01080.
[7] C.A. Ghiorghita, I.V. Platon, M.M. Lazar, M.V. Dinu, A.C. Aprotosoaie, Trends in polysaccharide-based hydrogels and their role in enhancing the bioavailability and bioactivity of phytocompounds, Carbohydr. Polym. 334 (2024), https://doi.org/10.1016/j.carbpol.2024.122033.
[8] E.M. Nsengiyumva, P. Alexandridis, Xanthan gum in aqueous solutions: fundamentals and applications, Int. J. Biol. Macromol. 216 (2022) 583–604, https://doi.org/10.1016/j.ijbiomac.2022.06.189.
[9] N.H.N. Do, Q.T. Truong, P.K. Le, A.C. Ha, Recent developments in chitosan hydrogels carrying natural bioactive compounds, Carbohydr. Polym. 294 (2022), https://doi.org/10.1016/j.carbpol.2022.119726.
[10] M. Abazari, T. Akbari, M. Hasani, E. Sharifikolouei, M. Raoufi, A. Foroumadi, M. Sharifzadeh, L. Firoozpour, M. Khoobi, Polysaccharide-based hydrogels containing herbal extracts for wound healing applications, Carbohydr. Polym. 294 (2022), https://doi.org/10.1016/j.carbpol.2022.119808.
[11] N. Jaradat, M. Hawash, M.N. Abualhasan, M. Qadi, M. Ghanim, E. Massarwy, S. A. Ammar, N. Zmero, M. Arar, F. Hussein, L. Issa, A. Mousa, A. Zarour, Spectral characterization, antioxidant, antimicrobial, cytotoxic, and cyclooxygenase inhibitory activities of Aloysia citriodora essential oils collected from two Palestinian regions, BMC Complement. Med. Ther. 21 (2021), https://doi.org/10.1186/s12906-021-03314-1.
[12] S. Tammar, N. Salem, W. Aidi Wannes, H. Limam, S. Bourgou, N. Fares, S. Dakhlaoui, M. Hammami, K. Saber, G. Del Re, K. Msaada, Chemical profiling and bioactivity of Aloysia citriodora essential oils from four localities in Tunisia, J. Essent. Oil Res. (2024), https://doi.org/10.1080/10412905.2024.2322592.
[13] V. Athanasiadis, T. Chatzimitakos, I. Makrygiannis, D. Kalompatsios, E. Bozinou, S.I. Lalas, Antioxidant-rich extracts from lemon verbena (Aloysia citrodora L.) leaves through response surface methodology, Oxygen 4 (2024) 1–19, https://doi.org/10.3390/oxygen4010001.
[14] L.M. Mena-Chacon, L. Quispe-Sanchez, A.F. Huaman-Pilco, E. Chávez-Chacón, R. Oblitas-Delgado, J. Basilio-Atencio, B. Aquino, N. Garcia, I. Yoplac, Lemon verbena (Aloysia citriodora) essential oil: Physicochemical characterization, microencapsulation, and application in starch-based bioplastics, Appl. Food Res. 5 (2025), https://doi.org/10.1016/j.afres.2025.101530.
[15] G.O. de Elguea-Culebras, E.M. Bravo, R. Sánchez-Vioque, Potential sources and methodologies for the recovery of phenolic compounds from distillation residues of Mediterranean aromatic plants. An approach to the valuation of by-products of the essential oil market – a review, Ind. Crops Prod. 175 (2022), https://doi.org/10.1016/j.indcrop.2021.114261.
[16] A. Skendi, M. Irakli, P. Chatzopoulou, E. Bouloumpasi, C.G. Biliaderis, Phenolic extracts from solid wastes of the aromatic plant essential oil industry: potential uses in food applications, Food Chem. Adv. 1 (2022), https://doi.org/10.1016/j.focha.2022.100065.
[17] M. Di Vito, A. Smolka, M.R. Proto, L. Barbanti, F. Gelmini, E. Napoli, M. G. Bellardi, P. Mattarelli, G. Beretta, M. Sanguinetti, F. Bugli, Is the antimicrobial activity of hydrolates lower than that of essential oils? Antibiotics 10 (2021) 88, https://doi.org/10.3390/antibiotics10010088.
[18] H.H.S. Almeida, I.P. Fernandes, J.S. Amaral, A.E. Rodrigues, M.-F. Barreiro, Unlocking the potential of hydrosols: transforming essential oil byproducts into valuable resources, Molecules 29 (2024) 4660, https://doi.org/10.3390/molecules29194660.
[19] J. Gonzalez-Rivera, B. Campanella, E. Pulidori, E. Bramanti, M.R. Tiné, L. Bernazzani, M. Onor, P. Bàrberi, C. Duce, C. Ferrari, From volatiles to solid wastes: towards the full valorization of lavender and rosemary by simultaneous in situ microwaves and ultrasounds irradiation extraction, Ind. Crop. Prod. 194 (2023), https://doi.org/10.1016/j.indcrop.2023.116362.
[20] H.H.S. Almeida, P.J.L. Crugeira, A. Santamaria-Echart, J.S. Amaral, T. C. Finimundy, L. Barros, A.E. Rodrigues, M.-F. Barreiro, Circular valorisation of essential oil post-distillation by-products for enhanced xanthan gum bioproduction and antimicrobial treatments against Staphylococcus aureus, Waste Biomass Valoriz. (2025), https://doi.org/10.1007/s12649-025-03302-3.
[21] A. Martínez-Ruvalcaba, E. Chornet, D. Rodrigue, Viscoelastic properties of dispersed chitosan/xanthan hydrogels, Carbohydr. Polym. 67 (2007) 586–595, https://doi.org/10.1016/j.carbpol.2006.06.033.

[22] O.M. Fahmy, R.A. Eissa, H.H. Mohamed, N.G. Eissa, M. Elsabahy, Machine learning algorithms for prediction of entrapment efficiency in nanomaterials, Methods 218 (2023) 133–140, https://doi.org/10.1016/j.ymeth.2023.08.008.
[23] M. Chen, Z. Hu, H. Zheng, J. Wang, X. Xu, Antimicrobial polysaccharide hydrogels embedded with methyl-β-cyclodextrin/thyme oil inclusion complexes for exceptional mechanical performance and chilled chicken breast preservation, Int. J. Biol. Macromol. 267 (2024), https://doi.org/10.1016/j.ijbiomac.2024.131586.
[24] Y. Guan, C. Yu, Z. Zang, X. Wan, A. Naeem, R. Zhang, W. Zhu, Chitosan/xanthan gum-based (hydroxypropyl methylcellulose-co-2-acrylamido-2-methylpropane sulfonic acid) interpenetrating hydrogels for controlled release of amorphous solid dispersion of bioactive constituents of Pueraria lobatae, Int. J. Biol. Macromol. 224 (2023) 380–395, https://doi.org/10.1016/j.ijbiomac.2022.10.131.
[25] Q. Yang, X. Cai, A. Yan, Y. Tian, M. Du, S. Wang, A specific antioxidant peptide: its properties in controlling oxidation and possible action mechanism, Food Chem. 327 (2020), https://doi.org/10.1016/j.foodchem.2020.126984.
[26] L. Barros, S. Oliveira, A.M. Carvalho, I.C.F.R. Ferreira, In vitro antioxidant properties and characterization in nutrients and phytochemicals of six medicinal plants from the Portuguese folk medicine, Ind. Crops Prod. 32 (2010) 572–579, https://doi.org/10.1016/j.indcrop.2010.07.012.
[27] I.P. Fernandes, J.S. Amaral, V. Pinto, M.J. Ferreira, M.F. Barreiro, Development of chitosan-based antimicrobial leather coatings, Carbohydr. Polym. 98 (2013) 1229–1235, https://doi.org/10.1016/j.carbpol.2013.07.030.
[28] J. Weißpflog, D. Vehlow, M. Müller, B. Kohn, U. Scheler, S. Boye, S. Schwarz, Characterization of chitosan with different degree of deacetylation and equal viscosity in dissolved and solid state – insights by various complimentary methods, Int. J. Biol. Macromol. 171 (2021) 242–261, https://doi.org/10.1016/j.ijbiomac.2021.01.010.
[29] A. Ćirić, Đ. Medarević, B. Čalija, V. Dobričić, M. Mitrić, L. Djekic, Study of chitosan/xanthan gum polyelectrolyte complexes formation, solid state and influence on ibuprofen release kinetics, Int. J. Biol. Macromol. 148 (2020) 942–955, https://doi.org/10.1016/j.ijbiomac.2020.01.138.
[30] S.M. Dadou, M.D. Antonijevic, B.Z. Chowdhry, A.A. Badwan, An Overview of Chitosan-Xanthan Gum Matrices as Controlled Release Drug Carriers, in: Chitin-Chitosan - Myriad Functionalities in Science and Technology, InTech, 2018, https://doi.org/10.5772/intechopen.76038.
[31] L.I.N. Tomé, M.S. Reis, H.C. de Sousa, M.E.M. Braga, Chitosan-xanthan gum PEC-based aerogels: a chemically stable PEC in scCO2, Mater. Chem. Phys. 287 (2022), https://doi.org/10.1016/j.matchemphys.2022.126294.
[32] O.A. Chat, P.A. Bhat, N. Nazir, A.A. Dar, Self-assembled systems based on surfactants and polymers as stabilizers for citral in beverages, in: Value-Added Ingredients and Enrichments of Beverages: Volume 14: The Science of Beverages, Elsevier, 2019, pp. 487–521, https://doi.org/10.1016/B978-0-12-816687-1.00015-1.
[33] A. Siemińska-Kuczer, M. Szymańska-Chargot, A. Zdunek, Recent advances in interactions between polyphenols and plant cell wall polysaccharides as studied using an adsorption technique, Food Chem. 373 (2022), https://doi.org/10.1016/j.foodchem.2021.131487.
[34] S. Afzal, M. Maswal, A.A. Dar, Rheological behavior of pH responsive composite hydrogels of chitosan and alginate: characterization and its use in encapsulation of citral, Colloids Surf. B Biointerfaces 169 (2018) 99–106, https://doi.org/10.1016/j.colsurfb.2018.05.002.
[35] R. Salihu, S.I. Abd Razak, N. Ahmad Zawawi, M. Rafiq Abdul Kadir, N. Izzah Ismail, N. Jusoh, M. Riduan Mohamad, N. Hasraf Mat Nayan, Citric acid: a green cross-linker of biomaterials for biomedical applications, Eur. Polym. J. 146 (2021), https://doi.org/10.1016/j.eurpolymj.2021.110271.
[36] C.E. Brunchi, M. Bercea, S. Morariu, M. Dascalu, Some properties of xanthan gum in aqueous solutions: effect of temperature and pH, J. Polym. Res. 23 (2016), https://doi.org/10.1007/s10965-016-1015-4.
[37] L. Zhang, J. Xu, Q. Wen, C. Ni, Preparation of xanthan gum nanogels and their pH/redox responsiveness in controlled release, J. Appl. Polym. Sci. 136 (2019), https://doi.org/10.1002/app.47921.
[38] M. Terta, G. Blekas, A. Paraskevopoulou, Retention of selected aroma compounds by polysaccharide solutions: a thermodynamic and kinetic approach, Food Hydrocoll. 20 (2006) 863–871, https://doi.org/10.1016/j.foodhyd.2005.08.011.
[39] H. Xue, X. Du, S. Fang, H. Gao, K. Xie, Y. Wang, J. Tan, The interaction of polyphenols-polysaccharides and their applications: a review, Int. J. Biol. Macromol. 278 (2024), https://doi.org/10.1016/j.ijbiomac.2024.134594.
[40] A. Theocharidou, S. Lousinian, A. Tsagkaris, I. Mourtzinos, C. Ritzoulis, Interactions between xanthan gum and phenolic acids, Int. J. Biol. Macromol. 273 (2024), https://doi.org/10.1016/j.ijbiomac.2024.133175.
[41] Q. Hu, Y. Luo, Polyphenol-chitosan conjugates: synthesis, characterization, and applications, Carbohydr. Polym. 151 (2016) 624–639, https://doi.org/10.1016/j.carbpol.2016.05.109.
[42] L. Xu, Q. Cai, X. Liu, P. Cai, C. Tian, X. Wu, C. Wang, B. Xiao, Instantaneous and reversible flocculation of Scenedesmus via chitosan and xanthan gum complexation, Bioresour. Technol. 390 (2023), https://doi.org/10.1016/j.biortech.2023.129899.
[43] N.S. Malik, M. Ahmad, M.U. Minhas, R. Tulain, K. Barkat, I. Khalid, Q. Khalid, Chitosan/xanthan gum based hydrogels as potential carrier for an antiviral drug: fabrication, characterization, and safety evaluation, Front. Chem. 8 (2020), https://doi.org/10.3389/fchem.2020.00050.
[44] I. Tagliaro, V. Radice, R. Nisticò, C. Antonini, Chitosan electrolyte hydrogel with low ice adhesion properties, Colloids Surf. A Physicochem. Eng. Asp. 700 (2024), https://doi.org/10.1016/j.colsurfa.2024.134695.
[45] N. Thombare, A. Mahto, D. Singh, A.R. Chowdhury, M.F. Ansari, Comparative FTIR characterization of various natural gums: a criterion for their identification, J. Polym. Environ. 31 (2023) 3372–3380, https://doi.org/10.1007/s10924-023-02821-1.
[46] S. Inphonlek, N. Niamsiri, P. Sunintaboon, C. Sirisinha, Chitosan/xanthan gum porous scaffolds incorporated with in-situ-formed poly(lactic acid) particles: their fabrication and ability to adsorb anionic compounds, Colloids Surf. A Physicochem. Eng. Asp. 603 (2020), https://doi.org/10.1016/j.colsurfa.2020.125263.
[47] A. Ćirić, J.M. Budinčić, Đ. Medarević, V. Dobričić, M. Rmandić, T. Barudžija, A. Malenović, L. Petrović, L. Djekic, Evaluation of chitosan/xanthan gum polyelectrolyte complexes potential for pH-dependent oral delivery of escin, Int. J. Biol. Macromol. 221 (2022) 48–60, https://doi.org/10.1016/j.ijbiomac.2022.08.190.
[48] R.M. Barbosa, D.N. da Rocha, R.F. Bombaldi de Souza, J.L. Santos, J.R. M. Ferreira, Â.M. Moraes, Cell-friendly chitosan-xanthan gum membranes incorporating hydroxyapatite designed for periodontal tissue regeneration, Pharmaceutics 15 (2023), https://doi.org/10.3390/pharmaceutics15020705.
[49] A.C. de Oliveira, R.M. Sabino, P.R. Souza, E.C. Muniz, K.C. Popat, M.J. Kipper, R. S. Zola, A.F. Martins, Chitosan/gellan gum ratio content into blends modulates the scaffolding capacity of hydrogels on bone mesenchymal stem cells, Mater. Sci. Eng. C 106 (2020), https://doi.org/10.1016/j.msec.2019.110258.
[50] H. Tian, Z. Lu, D. Li, J. Hu, Preparation and characterization of citral-loaded solid lipid nanoparticles, Food Chem. 248 (2018) 78–85, https://doi.org/10.1016/j.foodchem.2017.11.091.
[51] S.L. Recio-Cázares, P.I. Comett-Figueroa, R. Navarro-Amador, A. López-Malo, E. Palou, β-Cyclodextrin inclusion complex with essential oil from Lippia (Aloysia citriodora): preparation, physicochemical characterization, and its application on beef, ACS Food Sci. Technol. (2024), https://doi.org/10.1021/acsfoodscitech.4c00654.
[52] A. Dehghani, G. Bahlakeh, B. Ramezanzadeh, M. Ramezanzadeh, Aloysia citrodora leaves extract corrosion retardation effect on mild-steel in acidic solution: molecular/atomic scales and electrochemical explorations, J. Mol. Liq. 310 (2020), https://doi.org/10.1016/j.molliq.2020.113221.
[53] M. Krysa, M. Szymańska-Chargot, A. Zdunek, FT-IR and FT-Raman fingerprints of flavonoids – a review, Food Chem. 393 (2022), https://doi.org/10.1016/j.foodchem.2022.133430.
[54] H. Baltacıoğlu, C. Baltacıoğlu, I. Okur, A. Tanrıvermiş, M. Yalıç, Optimization of microwave-assisted extraction of phenolic compounds from tomato: characterization by FTIR and HPLC and comparison with conventional solvent extraction, Vib. Spectrosc. 113 (2021), https://doi.org/10.1016/j.vibspec.2020.103204.
[55] D. Sarmah, M.A. Rather, A. Sarkar, M. Mandal, K. Sankaranarayanan, N. Karak, Self-cross-linked starch/chitosan hydrogel as a biocompatible vehicle for controlled release of drug, Int. J. Biol. Macromol. 237 (2023), https://doi.org/10.1016/j.ijbiomac.2023.124206.
[56] I.A. Duceac, S. Coseri, Chitosan Schiff-base hydrogels—a critical perspective review, Gels 8 (2022), https://doi.org/10.3390/gels8120779.
[57] M. Nichifor, Role of hydrophobic associations in self-healing hydrogels based on amphiphilic polysaccharides, Polymers (Basel) 15 (2023), https://doi.org/10.3390/polym15051065.
[58] W. Dridi, N. Bordenave, Influence of polysaccharide concentration on polyphenol-polysaccharide interactions, Carbohydr. Polym. 274 (2021), https://doi.org/10.1016/j.carbpol.2021.118670.
[59] I.E. Raschip, R.N. Darie-Nita, N. Fifere, G.E. Hitruc, M.V. Dinu, Correlation between mechanical and morphological properties of polyphenol-laden xanthan gum/poly(vinyl alcohol) composite cryogels, Gels 9 (2023), https://doi.org/10.3390/gels9040281.
[60] E. Klein, J. Rimarčík, E. Senajová, A. Vagánek, J. Lengyel, Deprotonation of flavonoids severely alters the thermodynamics of the hydrogen atom transfer, Comput. Theor. Chem. 1085 (2016) 7–17, https://doi.org/10.1016/j.comptc.2016.04.004.
[61] R. De Piano, D. Caccavo, A.A. Barba, G. Lamberti, Polyelectrolyte hydrogels in biological systems: modeling of swelling and deswelling behavior, Chem. Eng. Sci. 279 (2023), https://doi.org/10.1016/j.ces.2023.118959.
[62] A.J. Sami, M. Khalid, T. Jamil, S. Aftab, S.A. Mangat, A.R. Shakoori, S. Iqbal, Formulation of novel chitosan guargum based hydrogels for sustained drug release of paracetamol, Int. J. Biol. Macromol. 108 (2018) 324–332, https://doi.org/10.1016/j.ijbiomac.2017.12.008.
[63] J. Potaś, E. Szymańska, A. Basa, A. Hafner, K. Winnicka, Tragacanth gum/chitosan polyelectrolyte complexes-based hydrogels enriched with xanthan gum as promising materials for buccal application, Materials 14 (2021) 1–15, https://doi.org/10.3390/ma14010086.
[64] K.M. Rao, D. Yeo, E. Kim, K.S.V.K. Rao, M.R.G.S. Chandra, S.S. Han, Xanthan gum and chitosan polyelectrolyte hydrogels with self-reinforcement of Zn+2 for wound dressing applications, Colloids Surf. A Physicochem. Eng. Asp. 699 (2024), https://doi.org/10.1016/j.colsurfa.2024.134550.
[65] F.A. Ngwabebhoh, O. Zandraa, R. Patwa, N. Saha, Z. Capáková, P. Saha, Self-crosslinked chitosan/dialdehyde xanthan gum blended hypromellose hydrogel for the controlled delivery of ampicillin, minocycline and rifampicin, Int. J. Biol. Macromol. 167 (2021) 1468–1478, https://doi.org/10.1016/j.ijbiomac.2020.11.100.
[66] W. Feng, Z. Wang, Tailoring the swelling-shrinkable behavior of hydrogels for biomedical applications, Adv. Sci. 10 (2023), https://doi.org/10.1002/advs.202303326.

[67] T.U. Wani, A.H. Pandith, F.A. Sheikh, Polyelectrolytic nature of chitosan: Influence on physicochemical properties and synthesis of nanoparticles, J Drug Deliv Sci Technol 65 (2021), https://doi.org/10.1016/j.jddst.2021.102730.
[68] R. Wang, C. Cheng, H. Wang, D. Wang, Swollen hydrogel nanotechnology: advanced applications of the rudimentary swelling properties of hydrogels, ChemPhysMater 3 (2024) 357–375, https://doi.org/10.1016/j.chphma.2024.07.006.
[69] M. Cheng, Y. Cui, Y. Guo, P. Zhao, J. Wang, R. Zhang, X. Wang, Design of carboxymethyl chitosan-reinforced pH-responsive hydrogels for on-demand release of carvacrol and simulation of release kinetics, Food Chem. 405 (2023), https://doi.org/10.1016/j.foodchem.2022.134856.
[70] A. Rahmatpour, A.H. Alizadeh, Biofilm hydrogel derived from physical crosslinking (self-assembly) of xanthan gum and chitosan for removing Cd2+, Ni2+, and Cu2+ from aqueous solution, Int. J. Biol. Macromol. 266 (2024), https://doi.org/10.1016/j.ijbiomac.2024.131394.
[71] A. Rezaei, F. Rafieian, S. Akbari-Alavijeh, M.S. Kharazmi, S.M. Jafari, Release of bioactive compounds from delivery systems by stimuli-responsive approaches; triggering factors, mechanisms, and applications, Adv. Colloid Interface Sci. 307 (2022), https://doi.org/10.1016/j.cis.2022.102728.
[72] H. Zhu, S. Chen, H. Duan, J. He, Y. Luo, Removal of anionic and cationic dyes using porous chitosan/carboxymethyl cellulose-PEG hydrogels: optimization, adsorption kinetics, isotherm and thermodynamics studies, Int. J. Biol. Macromol. 231 (2023), https://doi.org/10.1016/j.ijbiomac.2023.123213.
[73] F. Zhang, S. Zhang, S. Cui, X. Jing, Y. Feng, S. Coseri, Rapid self-healing carboxymethyl chitosan/hyaluronic acid hydrogels with injectable ability for drug delivery, Carbohydr. Polym. 328 (2024), https://doi.org/10.1016/j.carbpol.2023.121707.
[74] S.A.P. Siboro, D.S.B. Anugrah, K. Ramesh, S.H. Park, H.R. Kim, K.T. Lim, Tunable porosity of covalently crosslinked alginate-based hydrogels and its significance in drug release behavior, Carbohydr. Polym. 260 (2021), https://doi.org/10.1016/j.carbpol.2021.117779.
[75] P. Kalyani, M. Khandelwal, Drug release kinetics from in-situ modulated agar/chitosan-bacterial cellulose patches for differently soluble drugs, Int. J. Biol. Macromol. 283 (2024), https://doi.org/10.1016/j.ijbiomac.2024.137602.
[76] E. Altan, N. Turker, O.A. Hindy, Z. Dirican, O.B. Ozakpinar, A.U. Demir, D. Kalaskar, S. Thakur, O. Gunduz, Investigation of 3D-printed chitosan-xanthan gum patches, Int. J. Biol. Macromol. 213 (2022) 259–267, https://doi.org/10.1016/j.ijbiomac.2022.05.158.
[77] L. Yu, Y. Shen, J. Jin, D. Zhang, R. Wan, J. Song, W. Dong, C. Dong, S. You, Fabrication of a poly(gallic acid) nanoparticle-reinforced chitosan/xanthan gum hydrogel for treating diabetic oral ulcers, Colloids Surf. A Physicochem. Eng. Asp. 721 (2025), https://doi.org/10.1016/j.colsurfa.2025.137247.
[78] S.E. Lastra-Ripoll, S.E. Quintana, L.A. García-Zapateiro, Yogurt enriched with mango peel extracts (*Mangifera indica*) in chitosan–xanthan gum dispersions: physicochemical, rheological, stability, and antioxidant activity, Fluids 8 (2023), https://doi.org/10.3390/fluids8100259.
[79] I.P. Merlusca, C. Ibanescu, C. Tuchilus, M. Danu, L. Ionut Atanase, I.M. Popa, Characterization of neomycin-loaded xanthan-chitosan hydrogels for topical applications, Cellulose Chem. Technol. 53 (2018) 709–719, https://doi.org/10.35812/CelluloseChemTechnol.2019.53.69.
[80] D. Ramírez-Brewer, S.E. Quintana-Martinez, L.A. García-Zapateiro, Obtaining and characterization of natural extracts from mango (Mangifera Indica) peel and its effect on the rheological behavior in new mango kernel starch hydrogels, Food Chem. 462 (2025), https://doi.org/10.1016/j.foodchem.2024.140949.
[81] F. Cuomo, M. Cofelice, F. Lopez, Rheological characterization of hydrogels from alginate-based nanodispersion, Polymers (Basel) 11 (2019), https://doi.org/10.3390/polym11020259.
[82] L. Tavares, C.P. Zapata Noreña, H.L. Barros, S. Smaoui, P.S. Lima, M. Marques de Oliveira, Rheological and structural trends on encapsulation of bioactive compounds of essential oils: a global systematic review of recent research, Food Hydrocoll. 129 (2022), https://doi.org/10.1016/j.foodhyd.2022.107628.
[83] S. Chou, X. Meng, H. Cui, S. Zhang, H. Wang, B. Li, Rheological and pasting properties of maize, wheat and rice starch as affected by apple polyphenols, Int. J. Food Prop. 22 (2019) 1786–1798, https://doi.org/10.1080/10942912.2019.1671452.
[84] J. Yang, Y. Chen, L. Zhao, J. Zhang, H. Luo, Constructions and properties of physically cross-linked hydrogels based on natural polymers, Polym. Rev. 63 (2023) 574–612, https://doi.org/10.1080/15583724.2022.2137525.
[85] S.C. Briones, C.U. Mussagy, F.O. Farias, A. Córdova, Functional hydrogels in food applications: a review of crosslinking technologies, encapsulation trends, and emerging challenges, Polymers (Basel) 17 (2025), https://doi.org/10.3390/polym17212955.
[86] Q. He, X. Gao, Z. Wu, J. Zhu, H. Chen, X. Liu, X. Zhang, Robust, superabsorbent and antibacterial polysaccharide-based hybrid-network hydrogels for wound repair, Int. J. Biol. Macromol. 279 (2024), https://doi.org/10.1016/j.ijbiomac.2024.134626.
[87] M. Chelu, J.M. Calderon Moreno, A.M. Musuc, M. Popa, Natural regenerative hydrogels for wound healing, Gels 10 (2024), https://doi.org/10.3390/gels10090547.
[88] F. Rashid, P. Carter, S. Childs, Overview of hydrogels and the use of hyaluronic acid-based hydrogels in pharmaceutical transdermal delivery systems and topical cosmetic skin applications, Cosmetics 12 (2025) 265, https://doi.org/10.3390/cosmetics12060265.
[89] K. Zainab, H.M. Tahir, A. Ali, S. Ali, A. Muzamil, F. Ijaz, A. Ghaffar, M.T. Ali, F. Munir, Formulation and evaluation of silk sericin and xanthan gum–based injectable hydrogels for the treatment of burn wound, Regen. Eng. Transl. Med. 11 (2025) 760–773, https://doi.org/10.1007/s40883-025-00397-x.
[90] C.F.V. Sousa, J. Borges, J.F. Mano, Injectable and self-healable supramolecular hydrogels assembled by quaternised chitosan/alginate polyelectrolyte complexation for sustained drug delivery and cell encapsulation, Biomater. Sci. 13 (2025) 3617–3632, https://doi.org/10.1039/d5bm00072f.
[91] H. Cui, Y. Wang, C. Li, X. Chen, L. Lin, Antibacterial efficacy of Satureja montana L. essential oil encapsulated in methyl-β-cyclodextrin/soy soluble polysaccharide hydrogel and its assessment as meat preservative, LWT 152 (2021), https://doi.org/10.1016/j.lwt.2021.112427.
[92] D.M. Suflet, M. Constantin, I.M. Pelin, I. Popescu, C.M. Rimbu, C.E. Horhogea, G. Fundueanu, Chitosan–oxidized pullulan hydrogels loaded with essential clove oil: synthesis, characterization, antioxidant and antimicrobial properties, Gels 10 (2024), https://doi.org/10.3390/gels10040227.
[93] L. Shi, W. Zhao, Z. Yang, V. Subbiah, H.A.R. Suleria, Extraction and characterization of phenolic compounds and their potential antioxidant activities, Environ. Sci. Pollut. Res. 29 (2022) 81112–81129, https://doi.org/10.1007/s11356-022-23337-6.
[94] H.M. Rashid, A.I. Mahmod, F.U. Afifi, W.H. Talib, Antioxidant and antiproliferation activities of lemon verbena (Aloysia citrodora): an in vitro and in vivo study, Plants 11 (2022), https://doi.org/10.3390/plants11060785.
[95] E. Christaki, I. Giannenas, E. Bonos, P. Florou-Paneri, Innovative Uses of Aromatic Plants as Natural Supplements in Nutrition, Elsevier Inc., 2020, https://doi.org/10.1016/b978-0-12-814700-9.00002-9.
[96] J.A.B. Peixoto, G. Álvarez-Rivera, A.S.G. Costa, S. Machado, A. Cifuentes, E. Ibáñez, M.B.P.P. Oliveira, R.C. Alves, Contribution of phenolics and free amino acids on the antioxidant profile of commercial lemon verbena infusions, Antioxidants 12 (2023), https://doi.org/10.3390/antiox12020251.
[97] R.S. Riseh, M. Hassanisaadi, M. Vatankhah, S.A. Babaki, E.A. Barka, Chitosan as a potential natural compound to manage plant diseases, Int. J. Biol. Macromol. 220 (2022) 998–1009, https://doi.org/10.1016/j.ijbiomac.2022.08.109.
[98] M.E. Abd El-Hack, M.T. El-Saadony, M.E. Shafi, N.M. Zabermawi, M. Arif, G. E. Batiha, A.F. Khafaga, Y.M. Abd El-Hakim, A.A. Al-Sagheer, Antimicrobial and antioxidant properties of chitosan and its derivatives and their applications: a review, Int. J. Biol. Macromol. 164 (2020) 2726–2744, https://doi.org/10.1016/j.ijbiomac.2020.08.153.
[99] H.E. Cortés-Ferré, T. Arredondo-Ochoa, M. Gaytán-Martínez, Polysaccharides-polyphenolic interactions: formation, functionality and applications, Trends Food Sci. Technol. 163 (2025), https://doi.org/10.1016/j.tifs.2025.105117.
[100] J.F. Fisher, S. Mobashery, Constructing and deconstructing the bacterial cell wall, Protein Sci. 29 (2020) 629–646, https://doi.org/10.1002/pro.3737.
[101] H. Ma, Y. Zhao, Z. Lu, R. Xing, X. Yao, Z. Jin, Y. Wang, F. Yu, Citral-loaded chitosan/carboxymethyl cellulose copolymer hydrogel microspheres with improved antimicrobial effects for plant protection, Int. J. Biol. Macromol. 164 (2020) 986–993, https://doi.org/10.1016/j.ijbiomac.2020.07.164.
[102] C. Du, S. Li, Y. Fan, Y. Lu, J. Sheng, Y. Song, Preparation of gelatin-chitosan bilayer film loaded citral nanoemulsion as pH and enzyme stimuli-responsive antibacterial material for food packaging, Int. J. Biol. Macromol. 254 (2024), https://doi.org/10.1016/j.ijbiomac.2023.127620.
[103] T.T. Hung, P.T. Trang, H. Viet, N.T.M. Lan, L.T.M. Ngan, T.T. Hieu, In vitro antimicrobial activity of hydrosol from Litsea cubeba (Lour.) Pers. against Helicobacter pylori and Candida albicans, Biomed. Res. Ther. 7 (2020) 3819–3828, https://doi.org/10.15419/bmrat.v7i6.610.
[104] H.H.S. Almeida, P.J.L. Crugeira, J.S. Amaral, A.E. Rodrigues, M.F. Barreiro, Disclosing the potential of Cupressus leylandii A.B. Jacks & Dallim, *Eucalyptus globulus* Labill., *Aloysia citrodora* Paláu, and *Melissa officinalis* L. hydrosols as eco-friendly antimicrobial agents, Nat. Prod. Bioprospect. 14 (2024), https://doi.org/10.1007/s13659-023-00417-9.
[105] E. Stoleru, R.P. Dumitriu, G.L. Ailiesei, C. Yilmaz, M. Brebu, Synthesis of bioactive materials by in situ one-step direct loading of Syzygium aromaticum essential oil into chitosan-based hydrogels, Gels 8 (2022), https://doi.org/10.3390/gels8040225.